ACR No. 3K05

NATIONAL ADVISORY COMMITTEE FOR AERONAUTICS

WARTIME REPORT

ORIGINALLY ISSUED
November 1943 as
Advance Confidential Report 3K05

WIND TUNNEL TESTS OF AILERONS AT VARIOUS SPEEDS

V - PRESSURE DISTRIBUTIONS OVER THE NACA 66,2-216 AND NACA 23012 AIRFOILS WITH VARIOUS BALANCES ON 0.20-CHORD AILERONS

By W. Letko and H. G. Denaci

Langley Memorial Aeronautical Laboratory
Langley Field, Va.

NACA

WASHINGTON

NATIONAL ADVISORY COMMITTEE FOR AERONAUTICS

ADVANCE CONFIDENTIAL REPORT

WIND TUNNEL TESTS OF AILERONS AT VARIOUS SPEEDS V - PRESSURE DISTRIBUTIONS OVER THE NACA 66,2-216 AND NACA 23012 AIRFOILS WITH VARIOUS BALANCES ON 0.20-CHORD AILERONS

By W. Letko and H. G. Denaci

SUMMARY

Pressure-distribution tests of an NACA 66,2-216, a = 1.0, airfoil, equipped with a blunt-nose-balance aileron and a sealed internal-balance aileron, and of an NACA 23012 airfoil, equipped with a Frise aileron and a blunt-nose-balance aileron, were made in the two-dimensional test section of the LMAL stability tunnel. The tests were made at various airspeeds corresponding to Mach numbers of approximately 0.20 to 0.47. The pressures were measured on the upper and lower surface at the midspans of the main airfoil and the aileron for several different aileron deflections at several angles of attack.

The data are presented in the form of pressure-distribution diagrams for the airfoil-aileron combinations and for the aileron alone and as curves of section coefficients which were obtained by integration of the pressure-distribution diagrams of the airfoil-aileron combinations.

INTRODUCTION

The forms of aileron balances in current use have given performance that was satisfactory according to previous airplane requirements. With the development of current combat airplanes, however, large increases in the speed and the wing area of these airplanes, together with the demand for high rolling velocities, have made it necessary to balance almost completely the hinge moments of ailerons in order that the ailerons can be deflected under all conditions of flight. This close balance,

together with compressibility effects, has caused overbalance of ailerons at high speeds on some existing aileron installations. It has been considered desirable, therefore, to reinspect certain of the currently used or recently proposed balance arrangements from these considerations.

The NACA is thus undertaking a study of some of the more promising aileron forms at higher speeds than those employed in previous developments. References 1 to 4 have reported the effect of speed on section hinge-moment coefficients and section lift coefficients of 0.20-chord ailerons equipped with blunt-nose and sealed internal balances on the NACA 66,2-216, a = 1.0, airfoil and with blunt-nose and Frise balances on the NACA 23012 airfoil. The present report, which is intended to supplement the information previously given, presents data primarily to show the effect of speed on the pressure distribution over the same wing and aileron combinations as presented in references 1 to 4.

Pressure-distribution diagrams have been given at Mach numbers of approximately 0.20 and 0.47 for the configuration of each aileron that is believed to be the most practical. Pressure-distribution diagrams for the aileron have been given to show the change in pressure distribution with changes of aileron configuration at a Mach number of 0.36. Curves of the section coefficients, which were obtained by integration of the pressure-distribution diagrams of the airfoil-aileron combinations, are given for the airfoil-aileron combinations and for the aileron alone.

SYMBOLS

The coefficients and symbols used in this report are defined as follows:

c_n airfoil section normal-force coefficient $\left(\frac{n}{qc}\right)$

$c_{m_{c/4}}$ airfoil section pitching-moment coefficient about the quarter-chord point of the airfoil $\left(\frac{m_{c/4}}{qc^2}\right)$

c_{n_a} aileron section normal force coefficient $\left(\frac{n_a}{qc_a}\right)$

c_{c_a} aileron section chord-force coefficient $\left(\frac{x_a}{qc_a}\right)$

c_{h_a} aileron section ~~hinge moment~~ coefficient $\left(\frac{h_a}{qc_a^2}\right)$

P pressure coefficient; local static pressure minus static pressure of the free stream divided by dynamic pressure (Ordinate of pressure distribution diagram)

P_c critical pressure coefficient, that is, the pressure coefficient corresponding to the local velocity of sound

where

n section normal force

$m_{c/4}$ section pitching moment about the quarter-chord point of airfoil

n_a aileron section normal force

x_a aileron section chord force (not including profile drag)

h_a aileron section hinge moment

q dynamic pressure $\left(\frac{1}{2}\rho V^2\right)$

V air velocity

ρ mass density of air

and

α_o angle of attack of airfoil for infinite aspect ratio

δ_a aileron angle with respect to airfoil

M Mach number

APPARATUS AND MODEL

Tests were made in the two-dimensional test section of the stability tunnel. Air velocities up to 400 miles per hour can be obtained in this test section, which is 6 feet high and 2.5 feet wide. Figure 1 is a photograph of the test section with a model in place.

The models investigated had NACA 66,2-216, a = 1.0, and NACA 23012 airfoil sections of 2-foot chord. Table I gives the airfoil ordinates. The main portion of the airfoil models was made of laminated mahogany. The ailerons (fig. 2), of 0.20 chord and of true contour, were made of steel. The nose pieces were made of wood on all but the internal-balance aileron, on which a steel nose piece was used. The cover plates of the internal-balance aileron were made of 1/8-inch sheet steel that was rolled to the airfoil contour. The vent gap was varied by using cover plates of different lengths. The seals used on the internal-balance and blunt-nose ailerons were made of impregnated cotton fabric and extended completely across the airfoil span. In order to prevent leakage at the ends of the internal-balance aileron, the clearance between the ends of the balance and the walls was kept at a minimum and sealed with grease.

The aileron was supported at the ends by ball bearings housed in steel end plates attached to the airfoil. The airfoil completely spanned the tunnel and was fixed into circular end disks which were flush with the tunnel walls with about 1/8-inch clearance between the aileron and these end disks.

The angle of attack was changed by rotating the end disks. Aileron angles were varied and set from outside the tunnel. Pressure orifices were located on the center lines of the airfoils and ailerons except when a small amount of stagger was necessary where the orifices were closely spaced, as at the leading edge of the airfoil and aileron. The pressure distribution was recorded by photographing a multiple-tube manometer.

TESTS

The pressure-distribution tests reported herein were made simultaneously with hinge-moment and lift tests for all the model configurations reported in references 1 to 4; however, only those records believed to be the most useful are presented.

Records were taken at airspeeds corresponding to Mach numbers of approximately 0.20, 0.36, and 0.47; the lowest Mach number corresponds to a Reynolds number of 2,800,000 and the highest to a Reynolds number of about

6,700,000. Figure 3 is a plot of Reynolds number based on standard atmospheric conditions against test Mach number. Tests were made at indicated angles of attack of -5°, 0°, 5°, and 10°. With the internal-balance aileron, however, pressure-distribution records were taken only at angles of attack of 0° and 10°. For each angle of attack, records were taken at the indicated aileron deflections of 0°, $\pm 5^\circ$, $\pm 10^\circ$, and $\pm 16^\circ$. The highest value of Mach number could not be attained at large angles of attack with large aileron deflections because of limited tunnel power.

PRECISION

Angles of attack were set to within $\pm 0.1^\circ$ and aileron angles, to within $\pm 0.3^\circ$. The indicated aileron angles, which are given in the pressure-distribution diagrams, differ slightly from the actual aileron angles because of a small torsional deflection between the aileron and aileron-angle indicator; the aileron angles given in the plots of aerodynamic coefficients, however, have been corrected for the torsional deflection.

Corrections for tunnel-wall effects were applied to the section normal force, the section pitching-moment coefficients, and the angle of attack. The corrections applied are:

$$c_n = [1 - \gamma (1 + 2\beta)]\, c_n'$$

$$c_{m_{c/4}} = (1 - 2\beta\gamma)\, c_{m_{c/4}}' + \frac{\gamma}{4} c_n'$$

$$\alpha_o = (1 + \gamma)\, \alpha_o'$$

where

$$\gamma = \frac{\pi^2}{48} \left(\frac{c}{h}\right)^2$$

$\beta = 0.304$ (theoretical factor for NACA 66,2-216, a = 1.0 airfoil)

$\beta = 0.237$ (theoretical factor for NACA 23012 airfoil)

h height of tunnel

c_n' measured normal-force coefficient

α_o' uncorrected or geometric angle of attack

$c_{m_{c/4}}'$ measured pitching-moment coefficient

The values used are:

For the NACA 66,2-216 airfoil

$$c_n = 0.963\ c_n'$$

$$c_{m_{c/4}} = 0.986\ c_{m_{c/4}}' + 0.006\ c_n'$$

For the NACA 23012 airfoil

$$c_n = 0.966\ c_n'$$

$$c_{m_{c/4}} = 0.989\ c_{m_{c/4}}' + 0.006\ c_n'$$

For both airfoils

$$\alpha_o = 1.023\ \alpha_o'$$

Although the effect of compressibility on these corrections has been neglected, this neglect is not believed to invalidate the conclusions given.

No corrections were applied to the section hinge-moment coefficients, aileron section chord-force coefficients, aileron section normal-force coefficients, or the pressure-distribution diagrams.

RESULTS AND DISCUSSION

Section Pressure Distribution

Pressure-distribution diagrams of the NACA 66,2-216, a = 1.0, airfoil, equipped with a blunt-nose-balance aileron and a sealed internal-balance aileron and of the NACA 23012 airfoil, equipped with a Frise aileron and a blunt-nose-balance aileron are given in figures 4 to 7, respectively. The pressure coefficients in these diagrams have been plotted perpendicular to the chord line of the airfoil for all aileron deflections. These diagrams, which are presented primarily to show the effect of increasing the airspeed on the pressure distribution, show that

the negative pressure coefficients increased with increase of speed, except where the pressure coefficients were greater than the critical pressure coefficient or where separation took place. The theoretical variation of the critical pressure coefficient with Mach number, obtained from equation 6(a) of reference 5, is given in figure 8. Values of critical pressure coefficient have been indicated on the pressure-distribution diagrams for only the condition where the local speed of sound has been reached or exceeded.

The internal-balance aileron (fig. 5) was the only aileron tested that had peak pressures on the aileron that were always lower than those on the wing portion of the airfoil at all altitudes and aileron deflections. This condition is important because, at low angles of attack, peak pressures on the aileron may determine the critical speed of the airfoil-aileron combination.

On the blunt-nose-balance ailerons, the peak pressure over the balance nose generally did not increase with increase in airspeed and in some cases decreased considerably (figs. 4 and 7). This phenomenon can be attributed to separation brought about by the projecting corners of the balance. Because the characteristic shape of the pressure-distribution diagram over the aileron changed from approximately triangular to rectangular when separation or stall occurred, the hinge-moment coefficients were greatly increased.

The peak pressures at the nose of the Frise aileron (fig. 6) were very high in the unstalled range of negative aileron deflections and were usually higher than the peak pressures on any of the other ailerons tested. The flow through the slot between the aileron and the wing caused wide variations of pressure over the upper surface of the aileron forward of the hinge. No large peak pressures were noted on the aileron at positive deflections.

In order to show the effect of changes in balance, nose radii, and gap width on the pressure distribution of the various airfoil-aileron combinations, figures 9 to 11 have been presented, which give only the pressure distribution of the aileron portion of the airfoil for a Mach number of 0.36.

At aileron angles other than neutral, the pressure distribution of the blunt-nose-balance ailerons was considerably changed because of changes of the balance-nose

radii. (See fig. 9(a).) The balance nose of the ailerons projecting into the air stream caused separation at small aileron angles. The unstalled range of the aileron was increased considerably by increasing the nose radii from 0 to 0.02c. Figure 9(b) shows that sealing the gap decreases the peak pressure at the nose of the aileron and also eliminates the irregularities in the pressure caused by flow through the gap.

Pressure-distribution diagrams of the sealed-internal-balance aileron on the 66,2-216, a = 1.0, airfoil with three vent gaps are given in figure 10. Because there is no flow across the balance of this aileron, the location of the ends of the cover plates, which is defined by the vent gap, determines the pressure available for balance. Increases in the vent gap generally reduced the pressure difference across the balance.

The effect of variations of the nose radius of the Frise aileron is shown in figure 11(a). At negative aileron deflections the smallest nose radius, 0.0012c, caused the flow to separate at a small deflection. At $\delta_a = -10^\circ$, the 0.0080c radius delayed the stall but more than doubled the peak pressure; further increase of the radius to 0.0150c decreased the peak pressure. Variations of the radii had considerably less effect at zero or positive aileron deflections than at negative deflections.

Variations in the pressure distribution caused by increasing the vent gap from 0.0055c to 0.0100c with the 0.0080c nose radius and by rounding the lower surface to a radius of 0.02c at the entrance of the slot, are shown in figure 11(b). (For convenience, this radius of the rounded wing block will be designated lower-surface radius on the figures.) At negative aileron angles, as the flow is increased through the slot by increasing the vent gap and rounding the wing block at the slot entrance, the peak pressure is decreased.

During the tests, the aileron deflection for a given angle of attack at which the peak pressures reached a maximum over the nose of the Frise aileron was determined and is given in table II. The highest peak pressure coefficients were obtained at low Mach numbers and the aileron angle at which the pressure coefficient was maximum decreased with increase of speed.

Section Loads and Moments

The section coefficients for the various airfoil–aileron combinations, which are given in figures 12 to 15, were obtained from an integration of the pressure–distribution diagrams given in figures 4 to 7. The chord–force coefficient of the aileron has been used in calculating the pitching–moment coefficient of the airfoil, although none of the diagrams in which the pressures were plotted parallel to the aileron chord have been presented. Because the chord–force was evaluated by integrating the pressure–distribution diagrams, the magnitude of these forces will be in error by an amount equal to the skin–friction forces, which have not been included.

Each aileron apparently stalled at some deflection that depended on the geometry of the aileron, on the angle of attack, and on the speed; and the curves of load and moment coefficients changed appreciably at the stall. In every case the unstalled range was decreased with increase of speed. The slope of the curves of load and moment coefficients in the unstalled range was generally increased with increase of speed.

CONCLUSIONS

The results of the present investigation of pressure–distributions over the NACA 66,2–216, a = 1.0, and NACA 23012 airfoils with various balances on 0.20 chord ailerons indicate the following general conclusions:

1. Increasing the airspeed from a Mach number of approximately 0.20 to 0.47 caused large changes in the pressure distribution over the airfoil and aileron. The negative pressure coefficients increased with increase of speed, except when the pressure coefficient was greater than the critical pressure coefficient or when separation occurred. The unstalled range of the ailerons tested decreased with increase of speed.

2. The unstalled range of the blunt–nose and Frise ailerons was appreciably increased by increasing the radius of the nose of the balance. The highest peak pressures at the nose of the balance were obtained with the Frise aileron.

3. Sealing the gap of the blunt-nose-balance ailerons decreased the peak pressure at the nose of the aileron and eliminated the irregularities in the pressure caused by flow through the gap.

4. The internal-balance aileron was the only aileron tested that had lower peak pressures on the aileron than on the airfoil at all attitudes and deflections. This condition is important because at low angles of attack peak pressures on the aileron may determine the critical speed of the airfoil-aileron combination.

Langley Memorial Aeronautical Laboratory,
National Advisory Committee for Aeronautics,
Langley Field, Va.

REFERENCES

1. Letko, W., Denaci, H. G., and Freed, C.: Wind-Tunnel Tests of Ailerons at Various Speeds. I - Ailerons of 0.20 Airfoil Chord and True Contour with 0.35 Aileron-Chord Extreme Blunt Nose Balance on the NACA 66,2-216 Airfoil. NACA ACR, No. 3F11, 1943.

2. Denaci, H. G., and Bird, J. D.: Wind-Tunnel Tests of Ailerons at Various Speeds. II - Ailerons of 0.20 Airfoil Chord and True Contour with 0.60 Aileron-Chord Sealed Internal Balance on the NACA 66,2-216 Airfoil. NACA ACR, No. 3F18, 1943.

3. Letko, W., and Kemp, W. B.: Wind-Tunnel Tests of Ailerons at Various Speeds. III - Ailerons of 0.20 Airfoil Chord and True Contour with 0.35 Aileron-Chord Frise Balance on the NACA 23012 Airfoil. NACA ACR, No. 3I14, 1943.

4. Letko, W., Hollingworth, T. A., and Anderson, R. A.: Wind-Tunnel Tests of Ailerons at Various Speeds. IV - Ailerons of 0.20 Airfoil Chord and True Contour with 0.35 Aileron-Chord Extreme Blunt-Nose Balance on the NACA 23012 Airfoil. NACA ACR No. 5H28, 1943.

5. Robinson, Russell G., and Wright, Ray H.: Estimation of Critical Speeds of Airfoils and Streamline Bodies. NACA ACR, March 1940.

TABLE I.- ORDINATES OF AIRFOILS

[Stations and ordinates in percent of airfoil chord]

NACA 66,2-216, a = 1.0, airfoil

Upper surface		Lower surface	
Station	Ordinate	Station	Ordinate
0	0	0	0
.401	1.230	.599	-1.130
.640	1.484	.860	-1.344
1.128	1.858	1.372	-1.644
2.362	2.560	2.638	-2.183
4.846	3.604	5.154	-2.972
7.340	4.428	7.660	-3.580
9.838	5.140	10.162	-4.106
14.845	6.276	15.155	-4.930
19.860	7.156	20.140	-5.564
24.879	7.844	25.121	-6.054
29.900	8.366	30.100	-6.422
34.924	8.736	35.076	-6.676
39.949	8.980	40.051	-6.838
44.974	9.092	45.026	-6.902
50.000	9.060	50.000	-6.854
55.025	8.875	54.975	-6.685
60.048	8.496	59.952	-6.354
65.067	7.862	64.933	-5.802
70.081	6.941	69.919	-4.997
75.087	5.860	74.913	-4.070
80.085	4.644	79.915	-3.052
85.075	3.395	84.925	-2.049
90.055	2.103	89.945	-1.069
95.028	.913	94.972	-.281
100.000	0	100.000	0

L.E. radius: 1.575

NACA 23012 airfoil

Station	Ordinates	
	Upper surface	Lower surface
0	-------	0
1.25	2.67	-1.23
2.5	3.61	-1.71
5.0	4.91	-2.26
7.5	5.80	-2.61
10	6.43	-2.92
15	7.19	-3.30
20	7.56	-3.97
25	7.60	-4.28
30	7.55	-4.46
40	7.14	-4.48
50	6.41	-4.17
60	5.47	-3.67
70	4.36	-3.00
80	3.08	-2.16
90	1.68	-1.23
95	.92	-.70
100	.13	-.13

L.E. radius: 1.58

Slope or radius through end of chord: 0.305

TABLE II.- MAXIMUM PEAK PRESSURE COEFFICIENTS AT NOSE OF FRISE AILERON

[Nose radius = 0.008c; vent gap = 0.0055c]

α_o (deg)	δ_a (deg)	Maximum peak pressure coefficient	M
−5.1	−14.0	−3.3	0.197
0	−15.3	−4.5	.196
0	−10.8	−3.1	.472
5.1	−15.3	−4.9	.196
5.1	−12.0	−3.4	.454
10.2	−17.0	−5.4	.196
10.2	−11.3	−3.7	.444

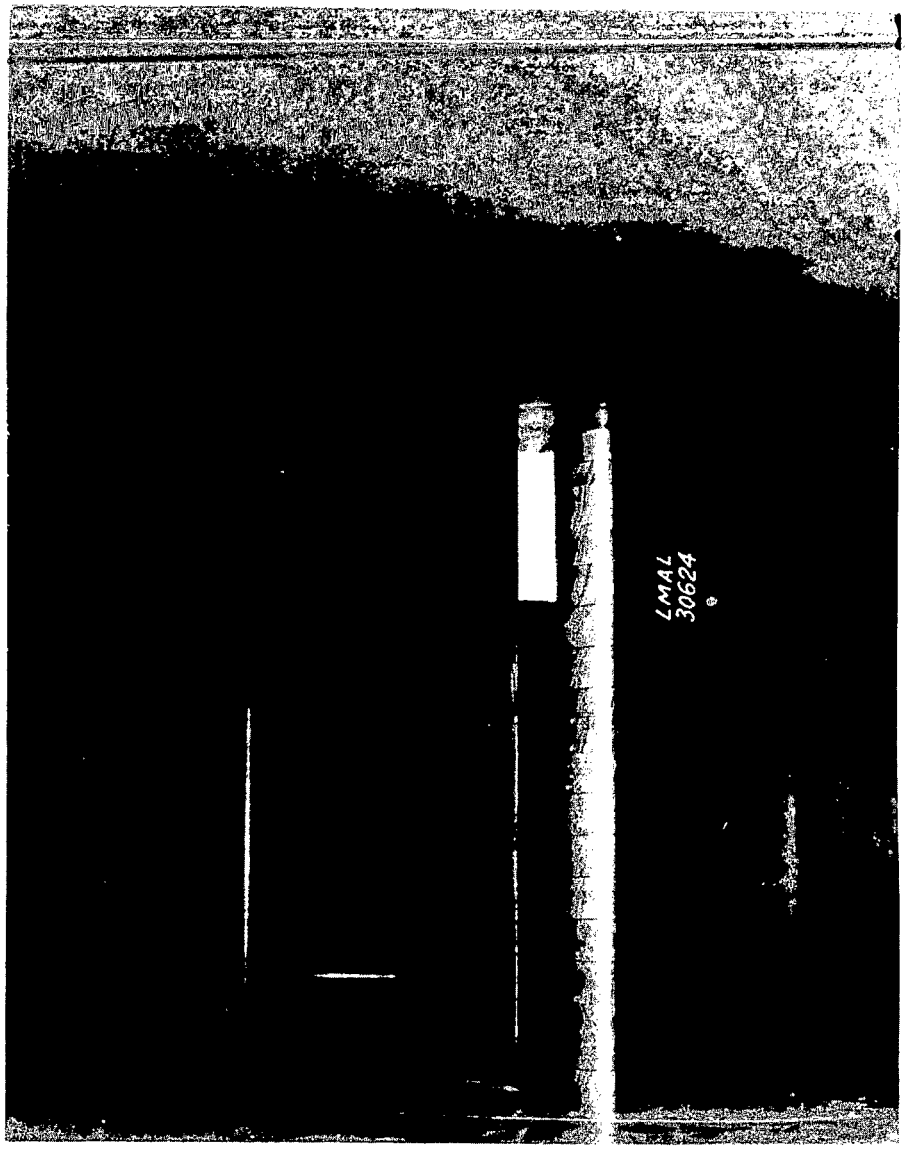

Figure 1.- Airfoil and aileron mounted in tunnel.

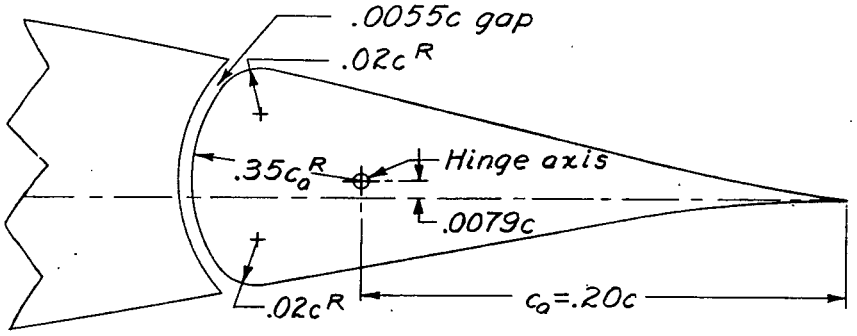

(a) Blunt-nose-balance aileron on the NACA 66,2-216, a=1.0 airfoil.

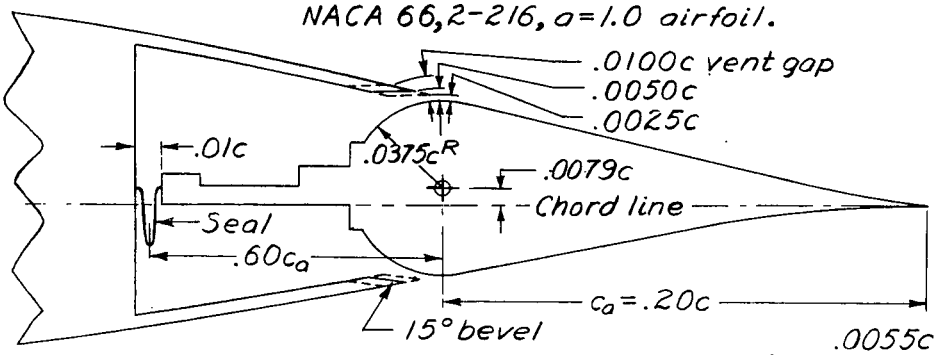

(b) Sealed-internal-balance aileron on the NACA 66,2-216 airfoil.

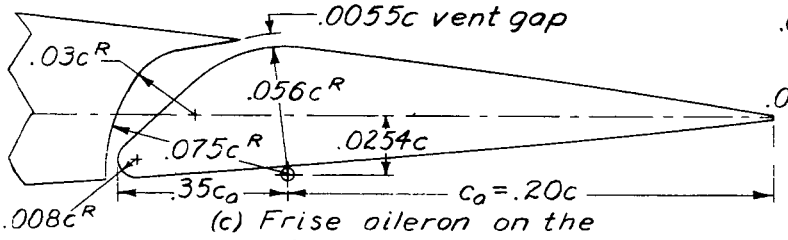

(c) Frise aileron on the NACA 23012 airfoil.

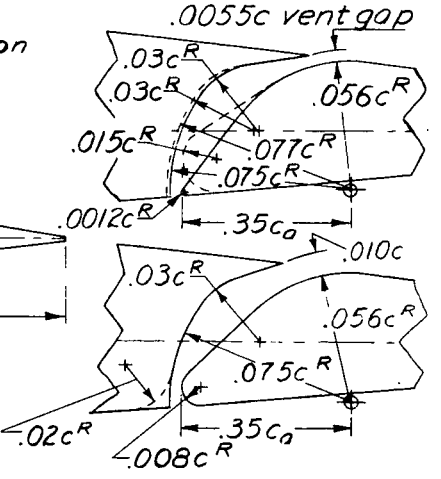

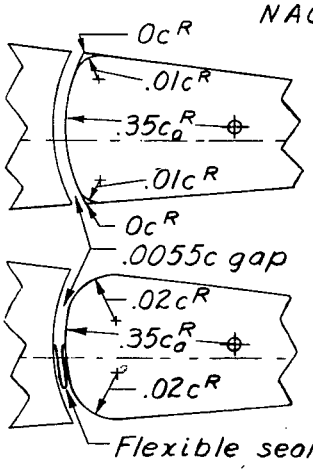

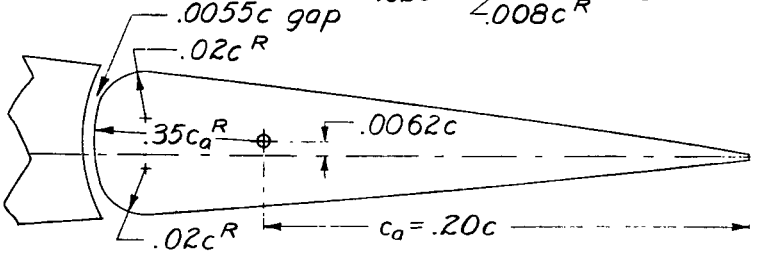

(d) Blunt-nose-balance aileron on the NACA 23012 airfoil.

Figure 2. — Sketch of ailerons. All ailerons are of true contour. c = 24.00 inches.

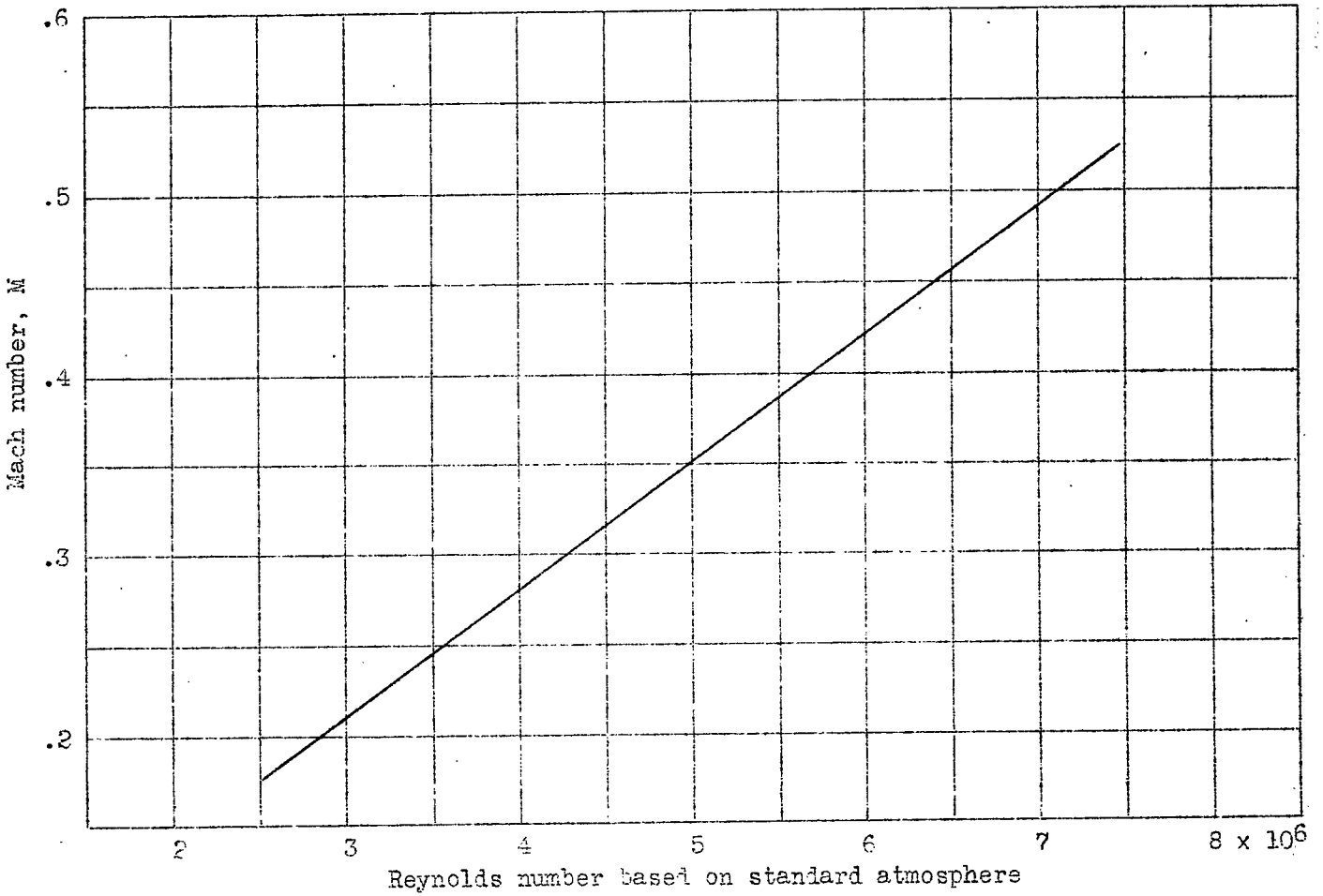

Figure 3.- Reynolds number for values of test Mach number for a 2-foot chord airfoil in the 2.5-by 6-foot test section of the stability tunnel.

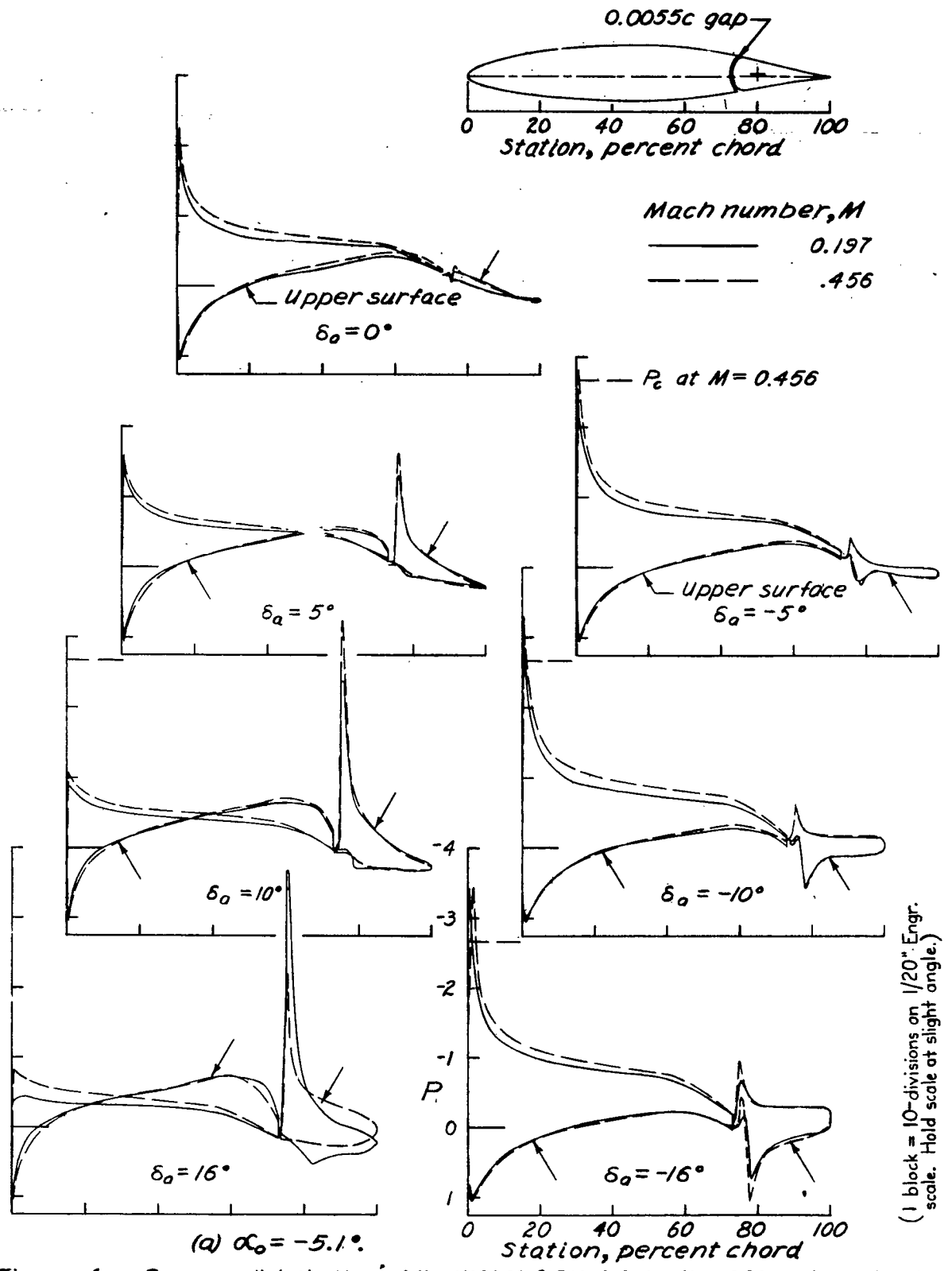

Figure 4. —Pressure distribution of the NACA 66, 2-216 airfoil with a 0.20c gileron having a blunt-nose balance of $0.35c_a$ and 0.02c balance-nose radii.

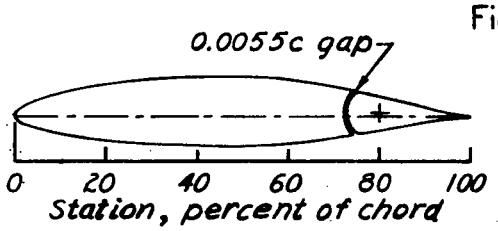

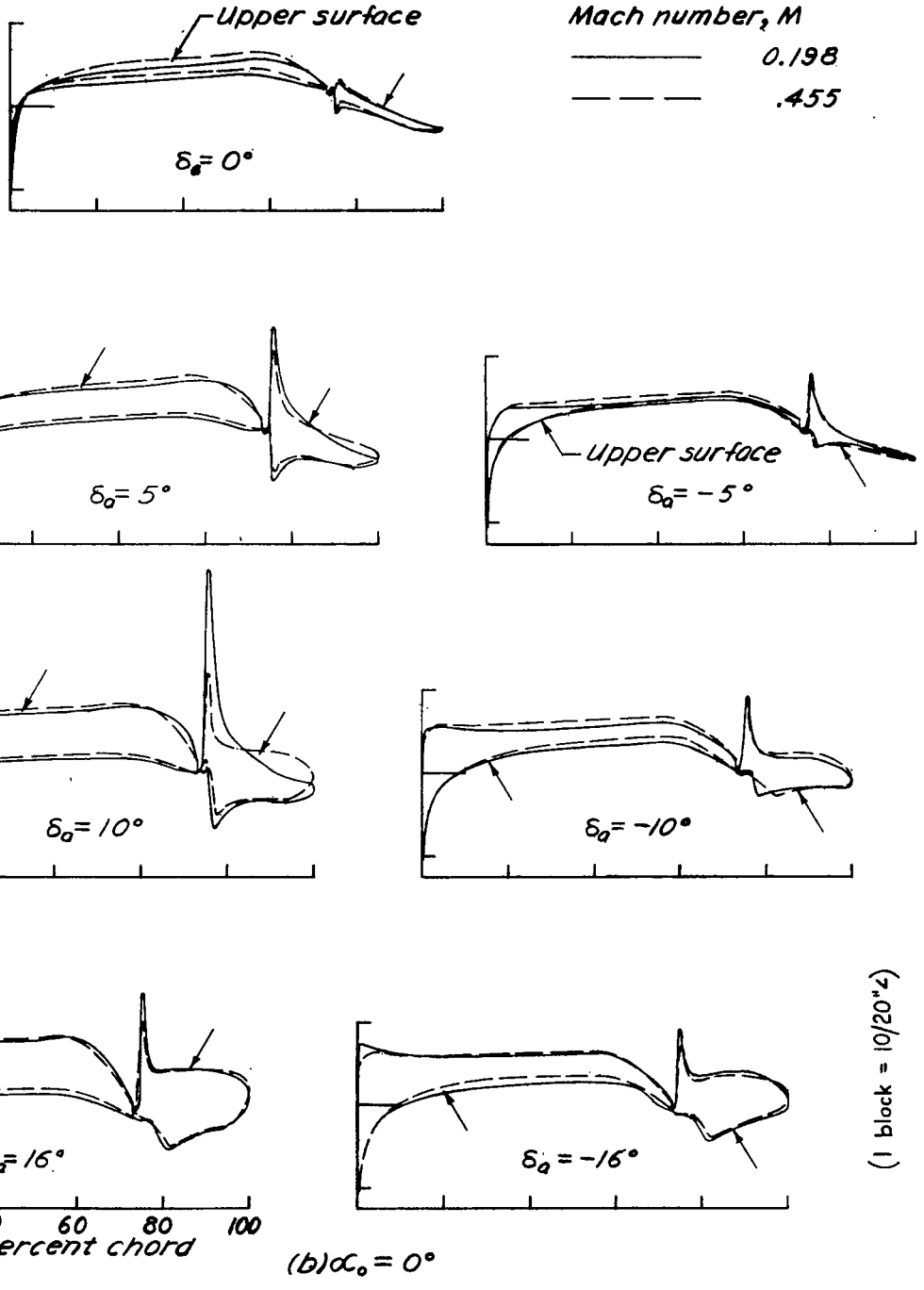

(b) $\alpha_o = 0°$

Figure 4. — Continued.

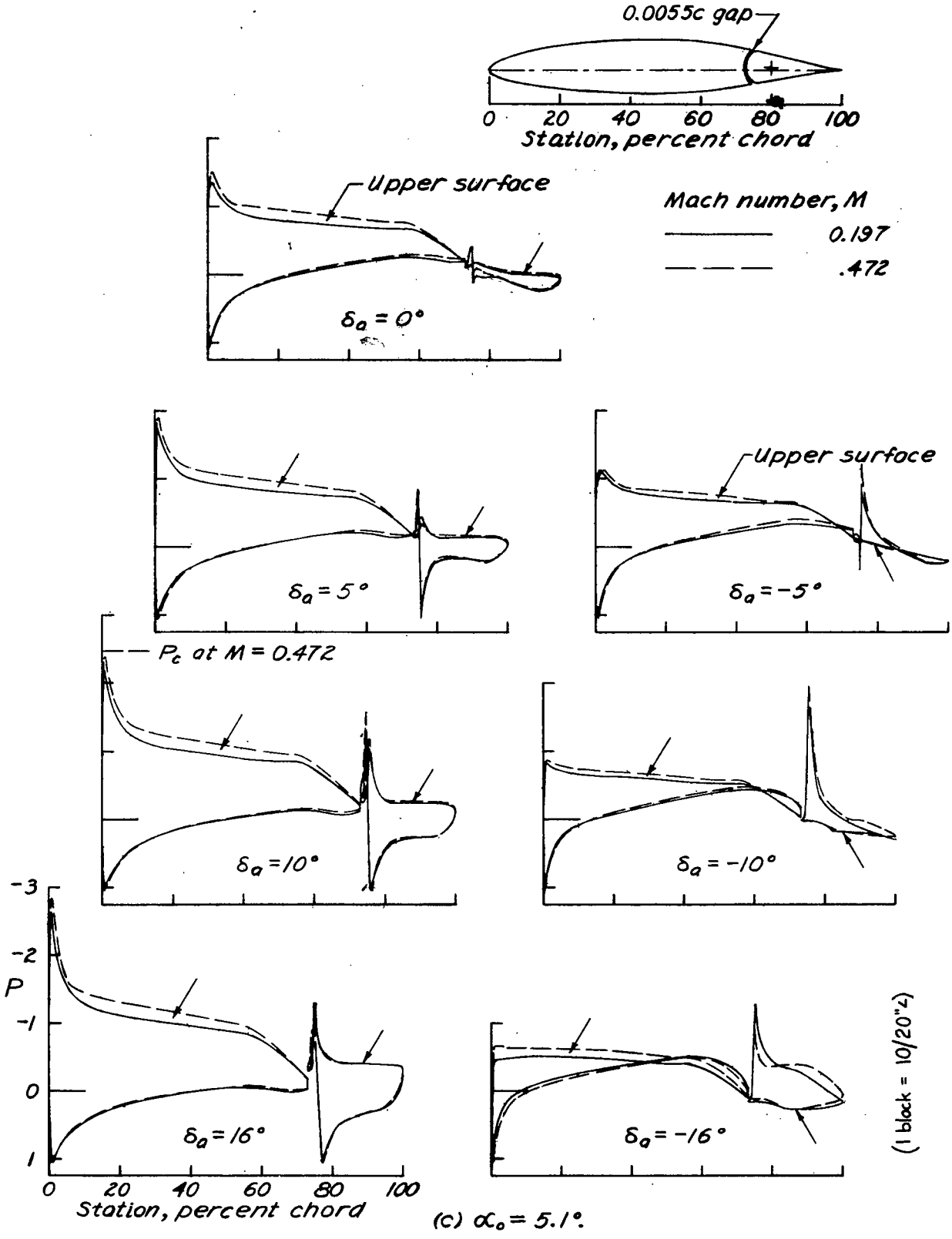

(c) $\alpha_o = 5.1°$.

Figure 4.—Continued.

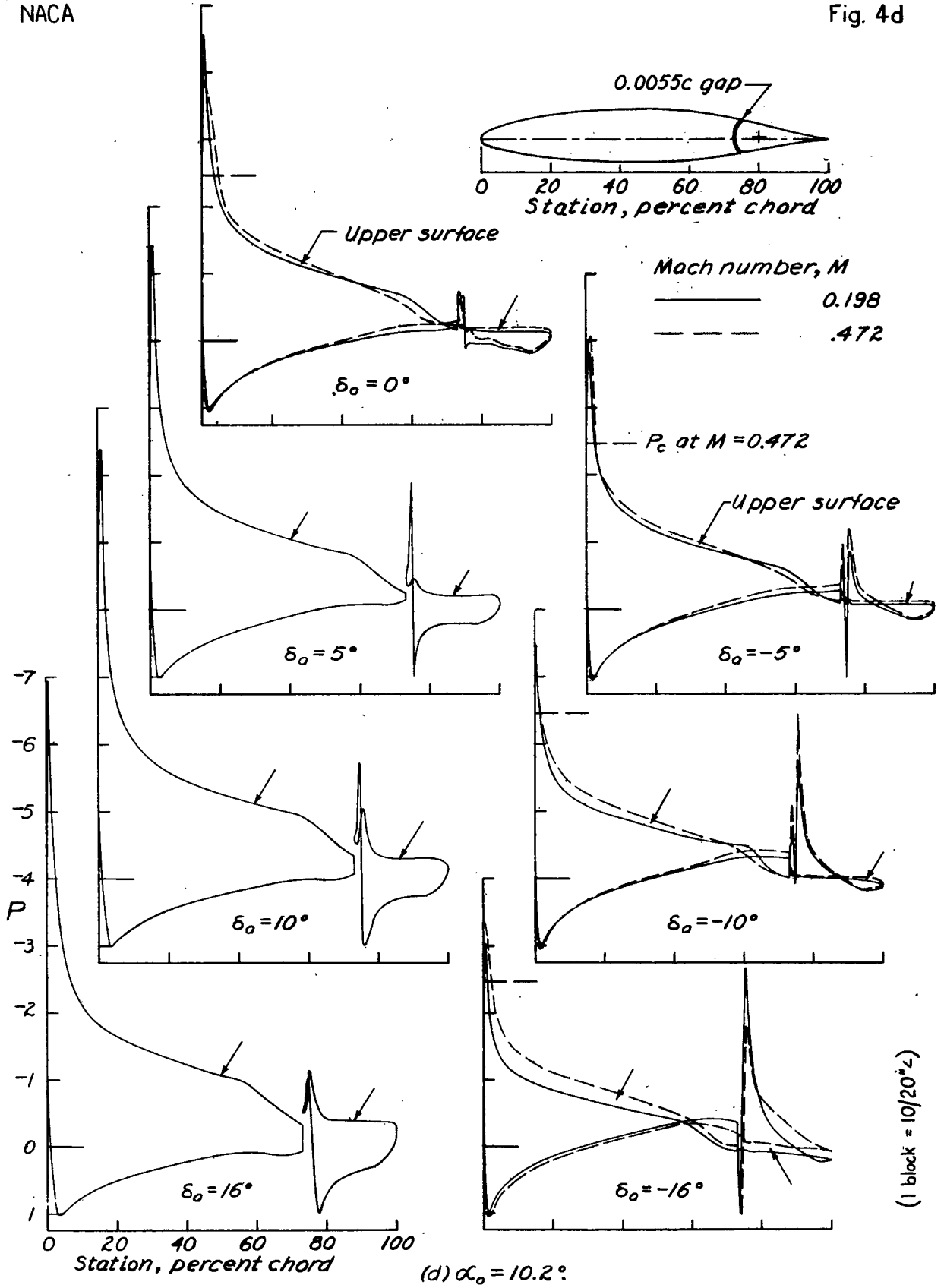

(d) $\alpha_o = 10.2°$

Figure 4. — Concluded.

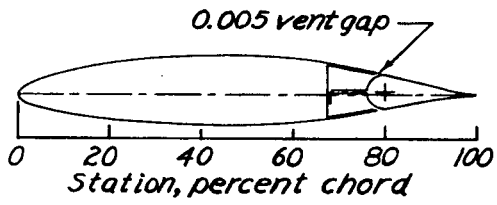

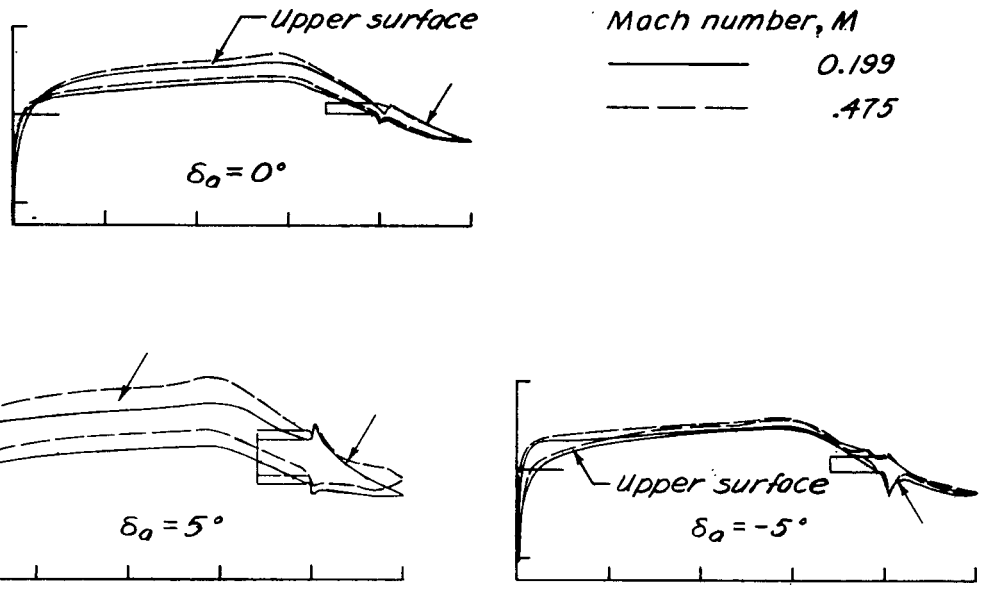

Figure 5. —Pressure distribution of the NACA 66,2-216 airfoil with a 0.20c aileron having an internal balance of 0.60 c_a.

NACA

Fig. 5b

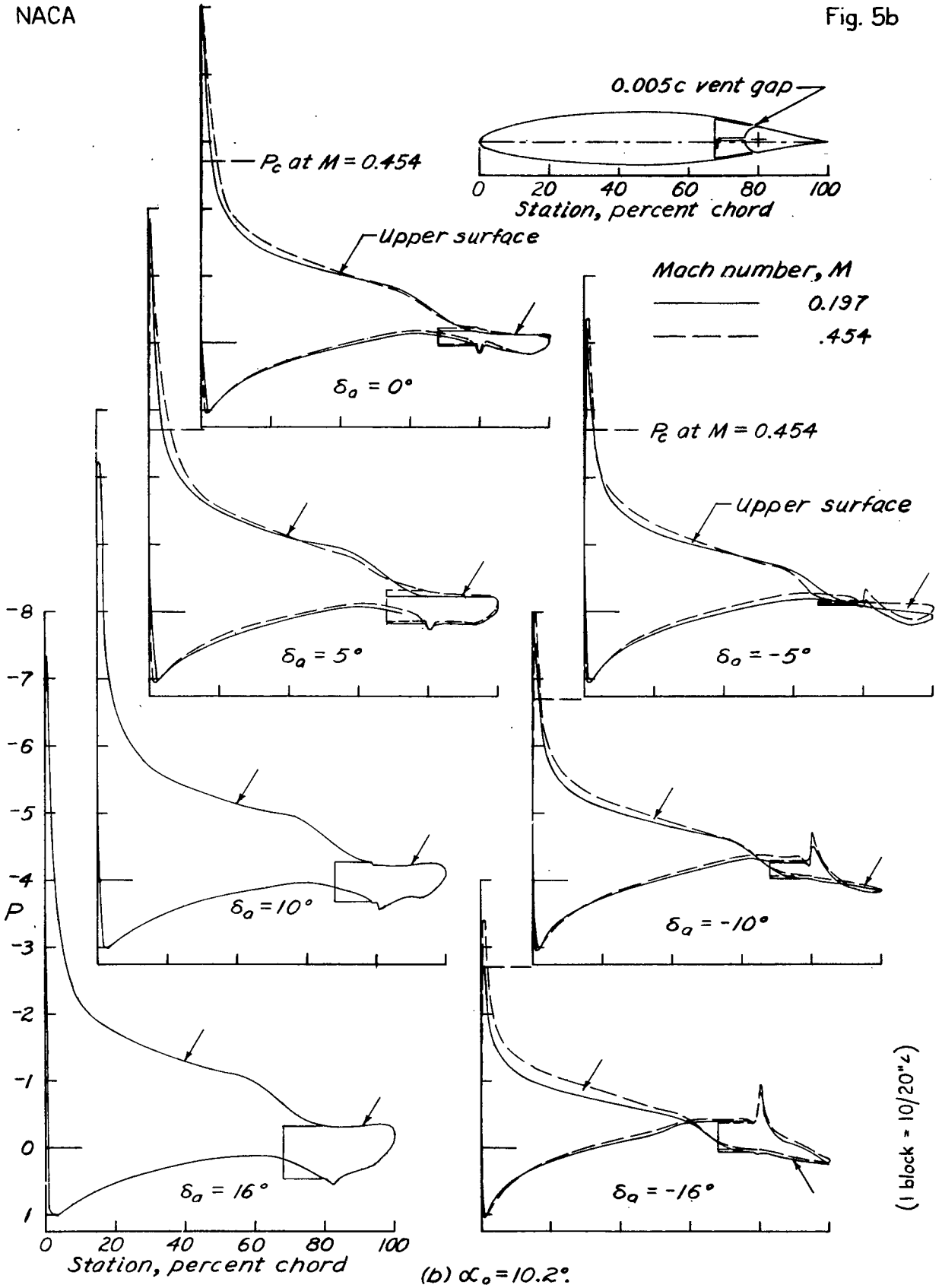

(b) α_o = 10.2°.

Figure 5.— Concluded.

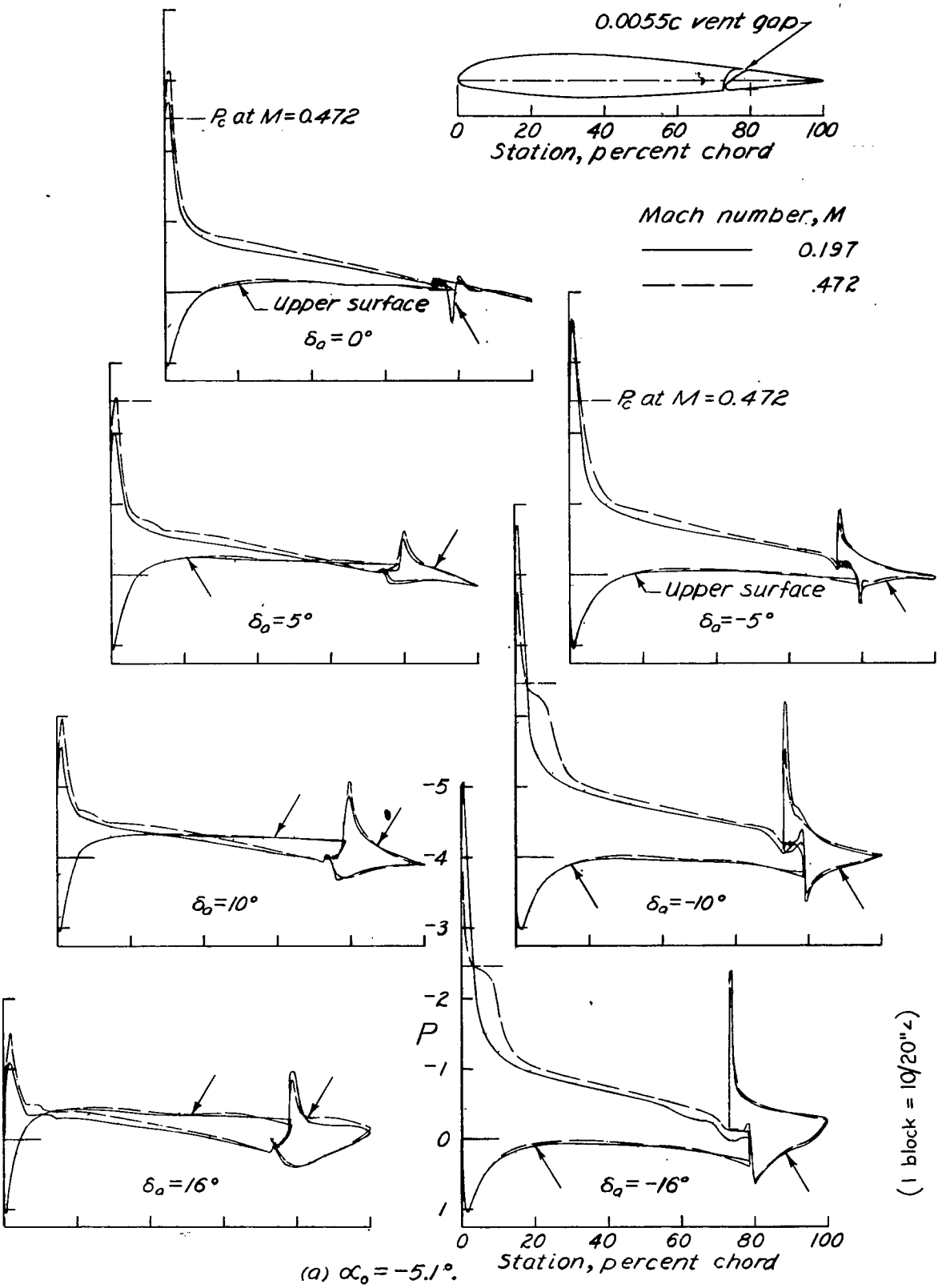

(a) $\alpha_0 = -5.1°$.

Figure 6. — Pressure distribution of the NACA 23012 airfoil with a 0.20c aileron having a Frise type balance of $0.35c_a$ and a 0.008c nose radius.

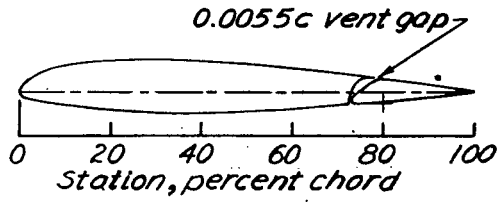

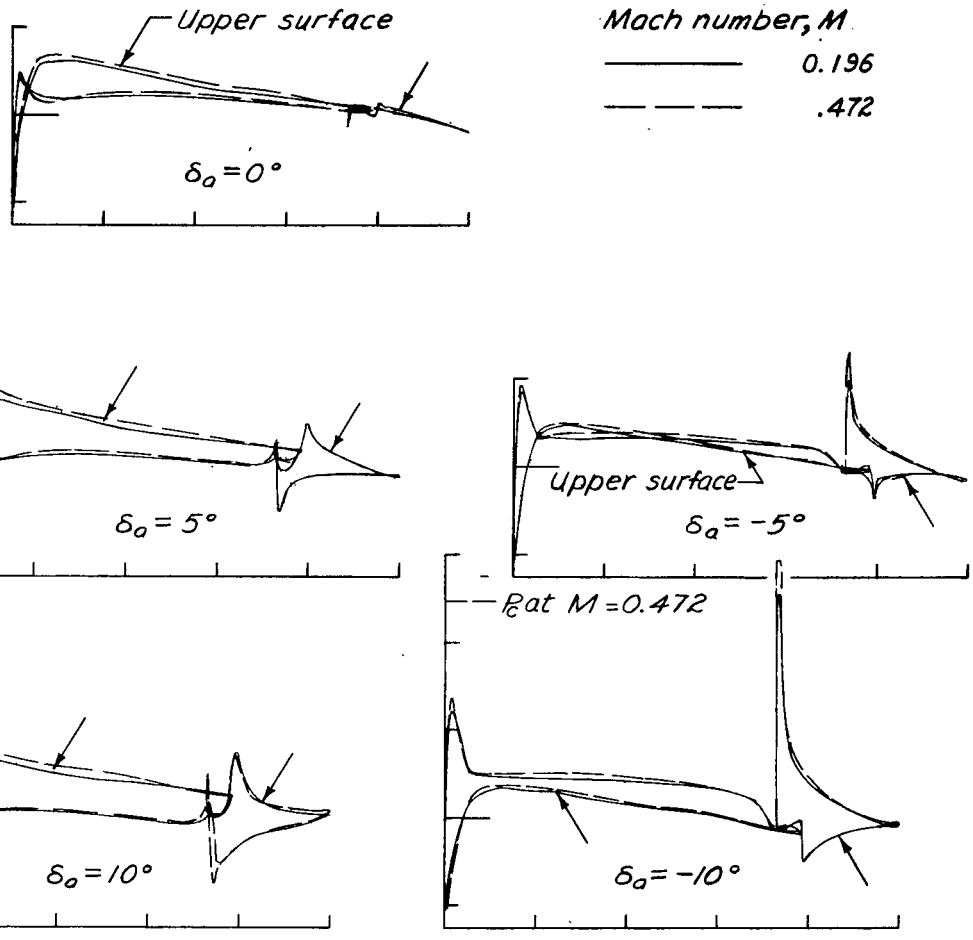

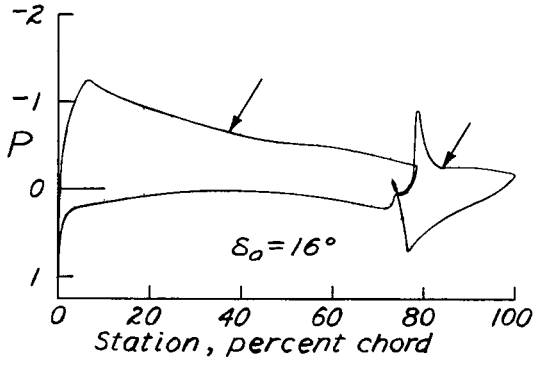

(b) $\alpha_o = 0°$

(1 block = 10/20")

Figure 6. — Continued.

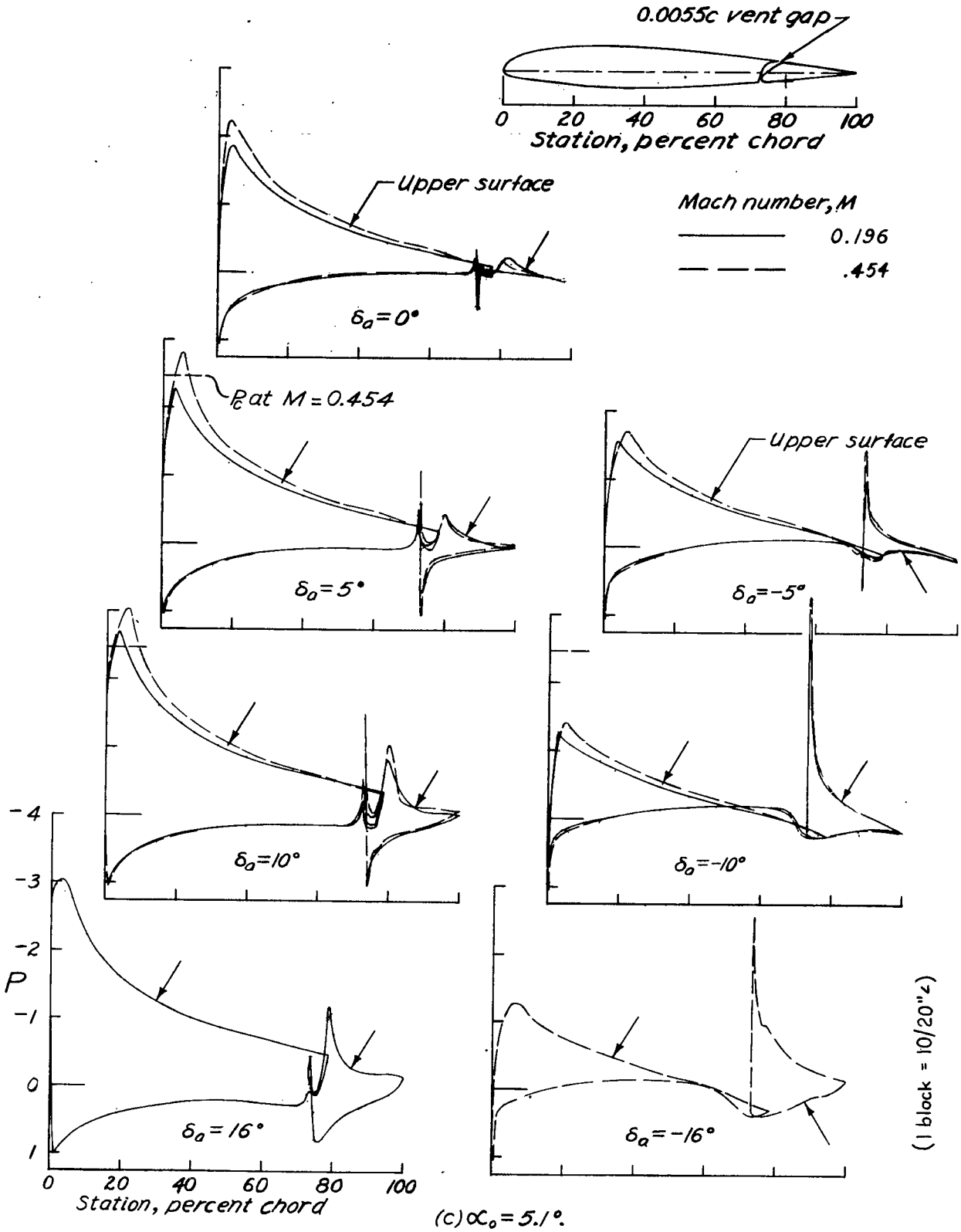

(c) $\alpha_o = 5.1°$.

Figure 6.— Continued.

NACA

Fig. 6d

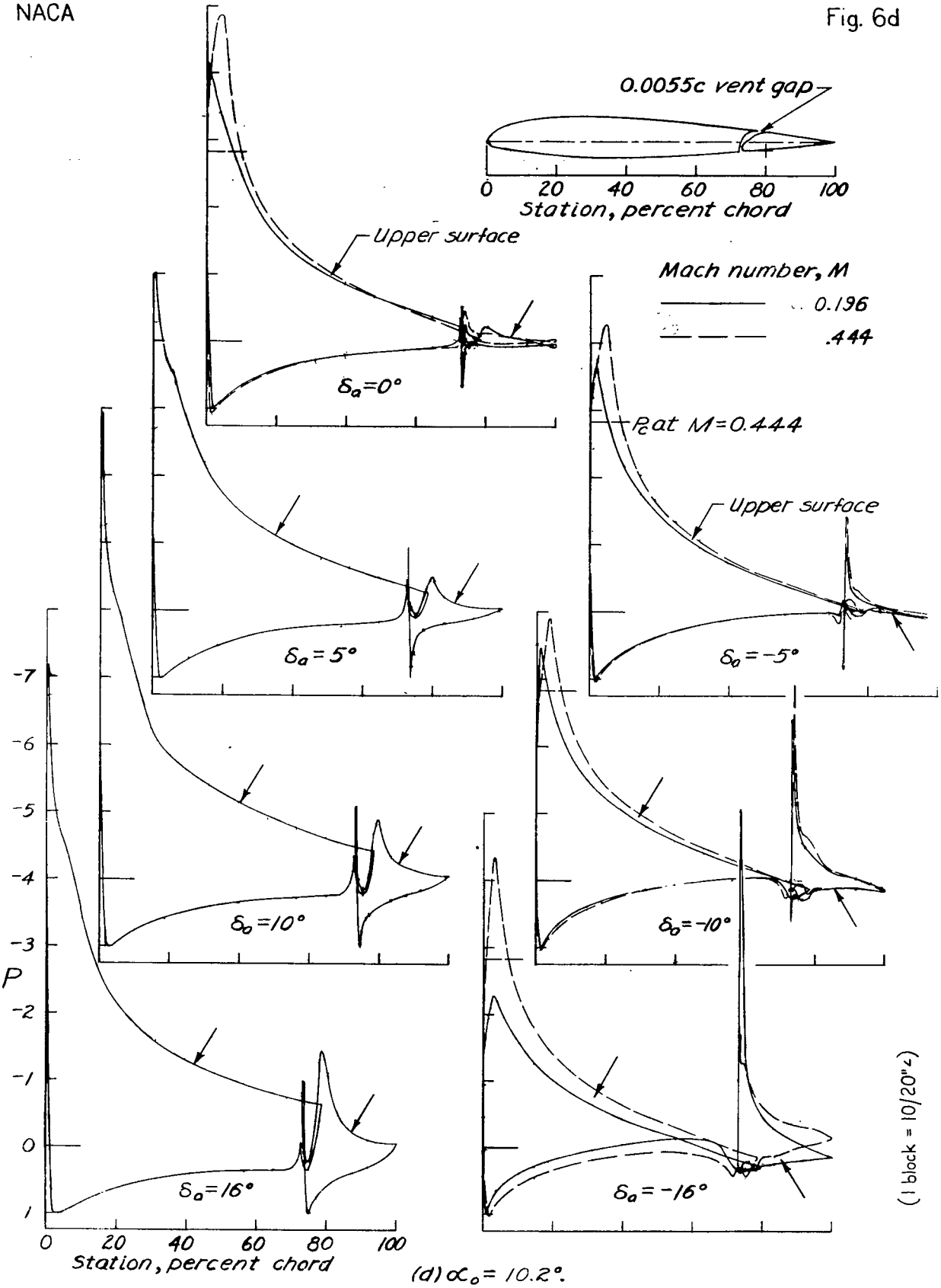

(d) $\alpha_o = 10.2°$.

Figure 6. — Concluded.

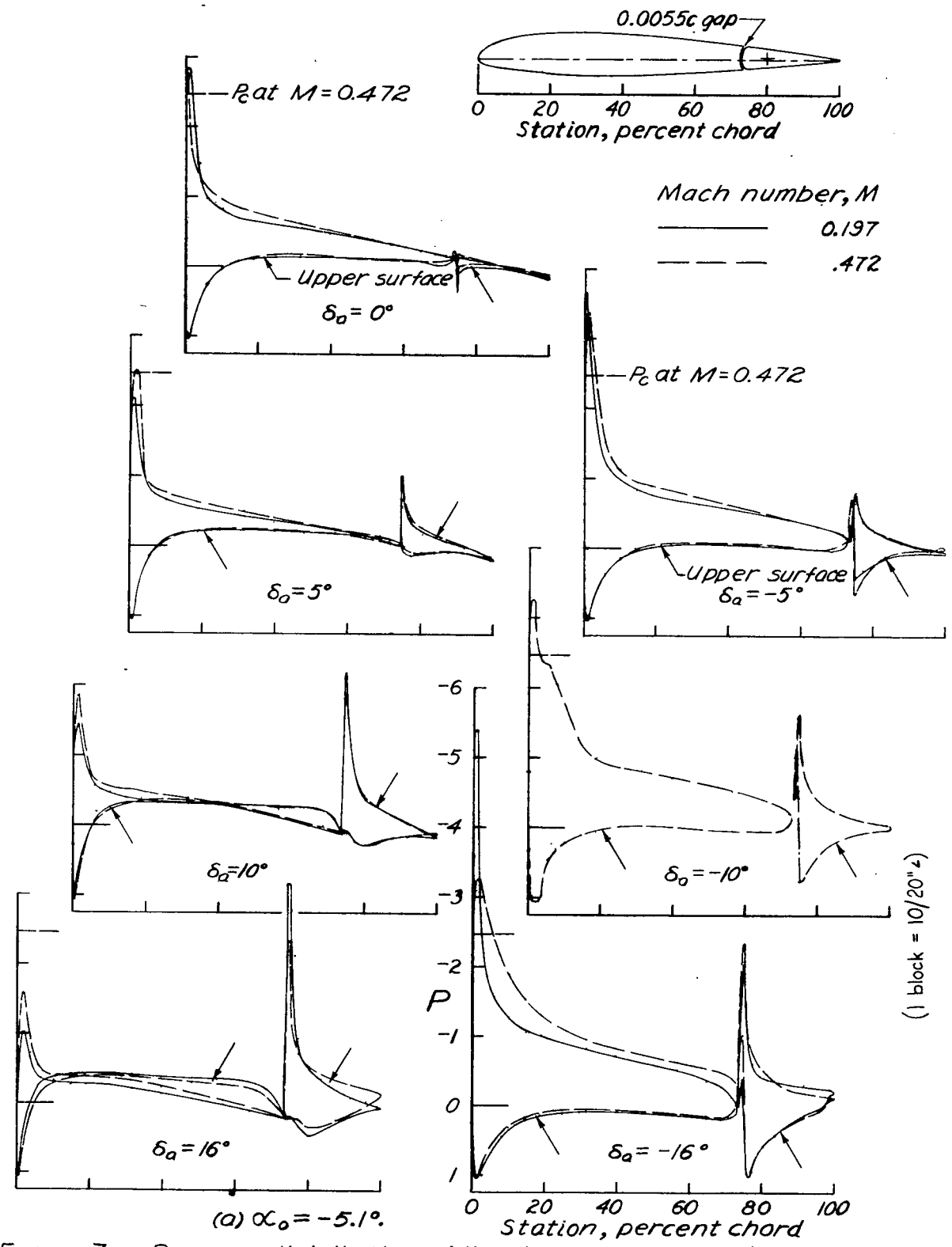

Figure 7. – Pressure distribution of the NACA 23012 airfoil with a 0.20c aileron having a blunt-nose balance of $0.35c_a$ and 0.02c balance-nose radii.

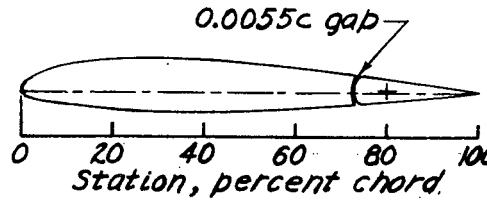

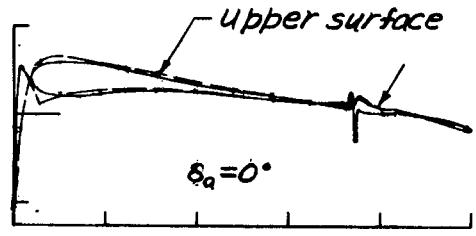

Mach number, M

0.196

.473

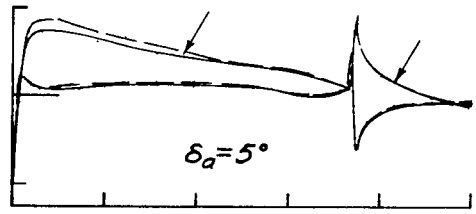

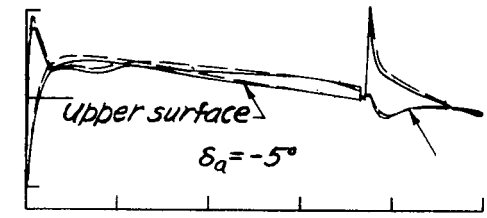

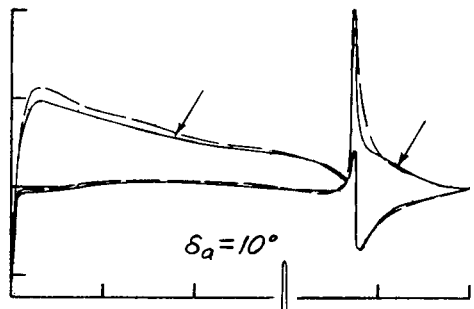

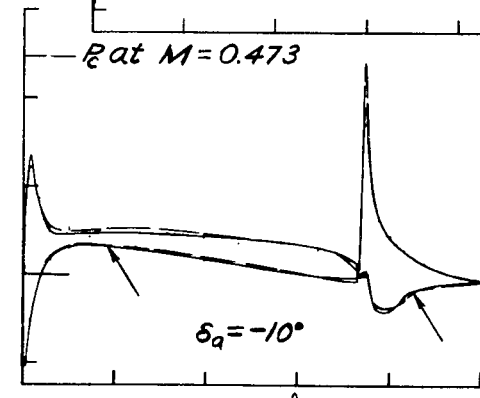

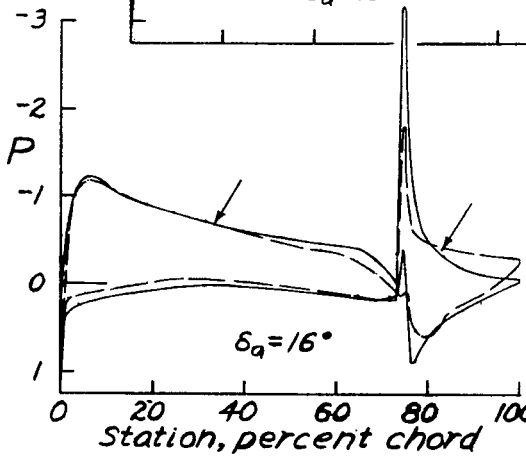

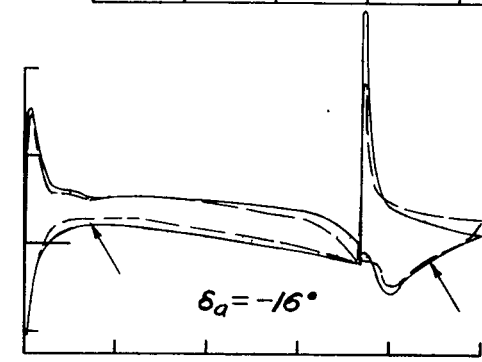

(1 block = 10/20")

(b) $\alpha_o = 0°$.

Figure 7. — Continued.

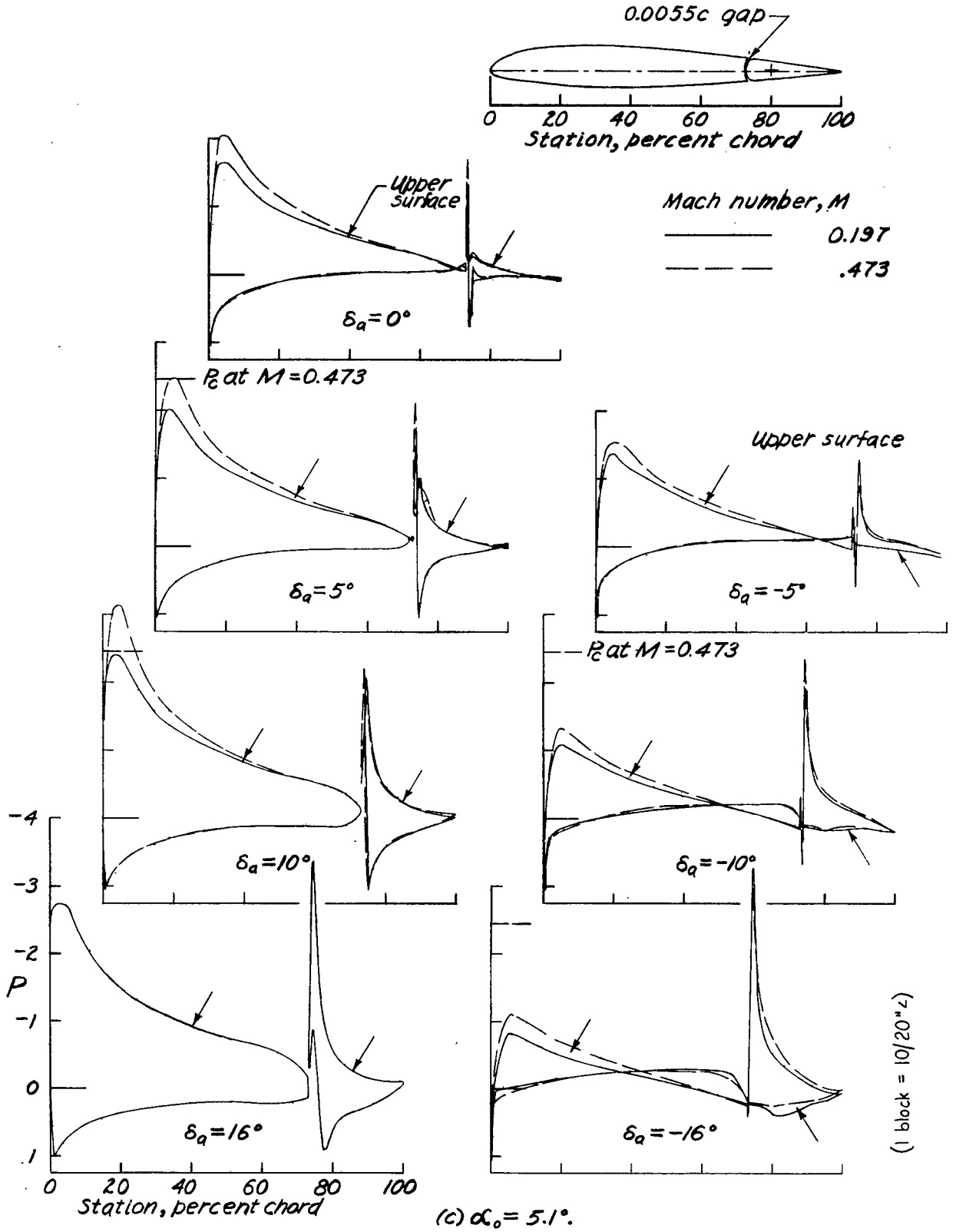

(c) $\alpha_o = 5.1°$.

Figure 7. —Continued.

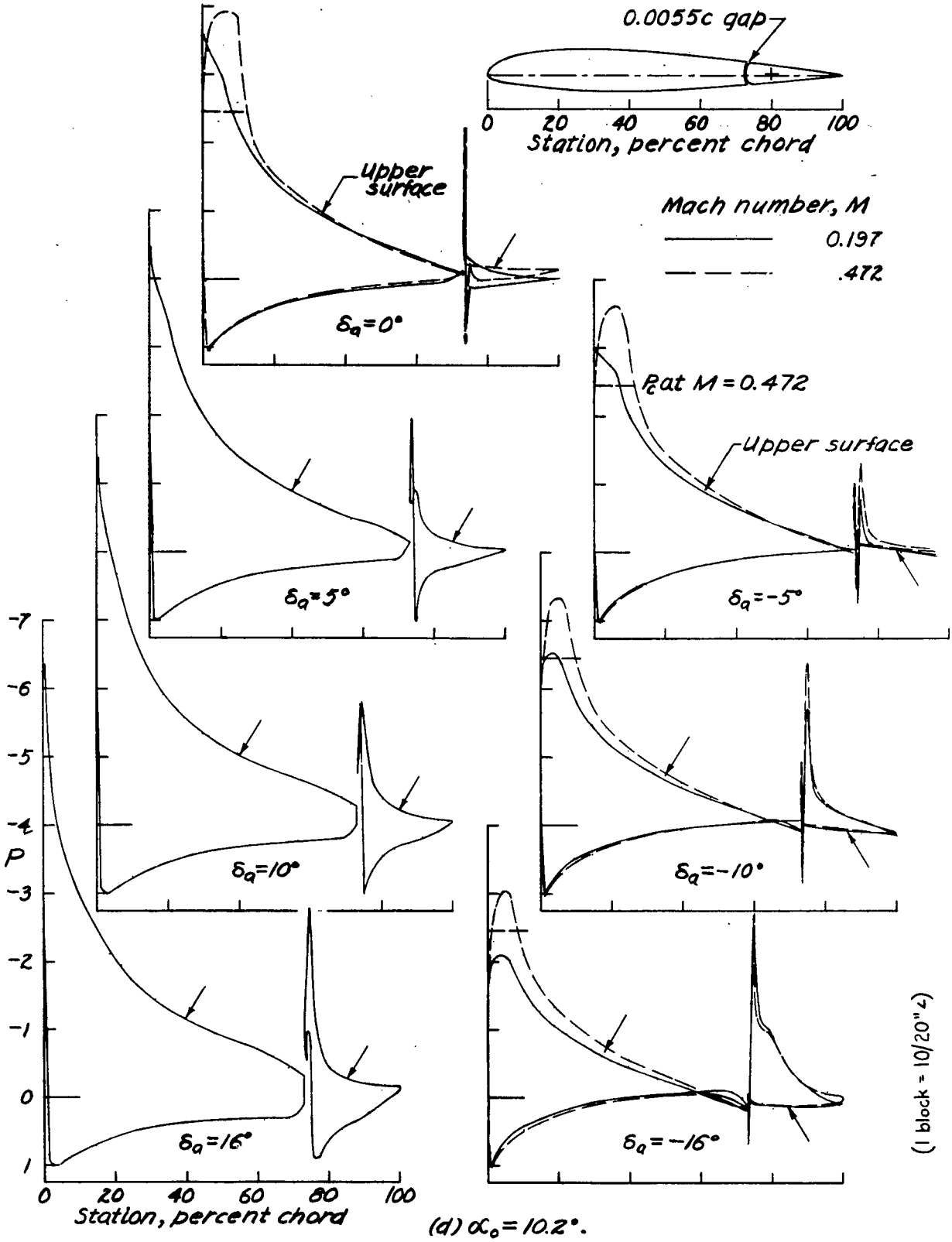

(d) $\alpha_o = 10.2°$.

Figure 7. — Concluded.

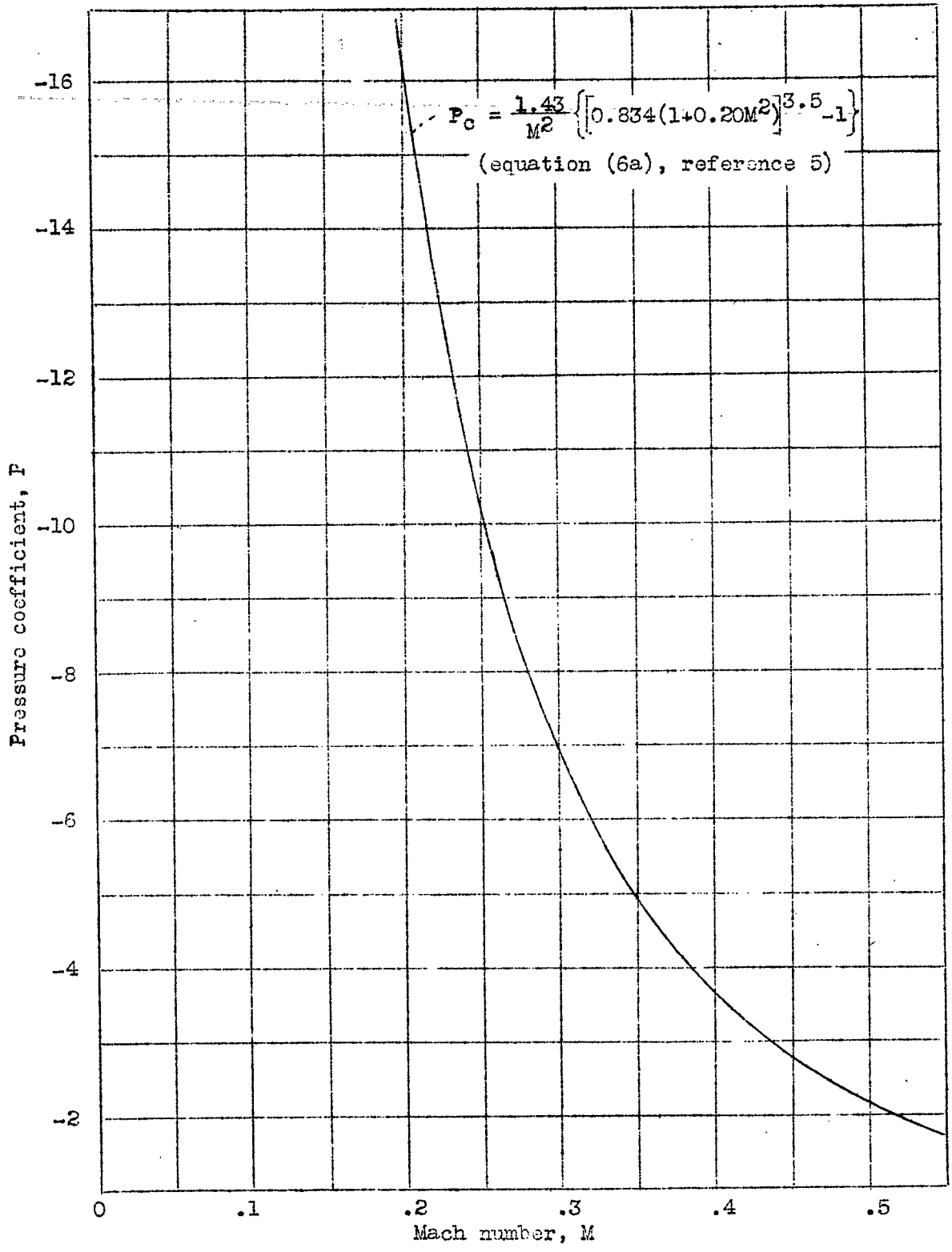

Figure 8.- Theoretical variation of critical-pressure coefficient with Mach number.

NACA

Fig. 9a

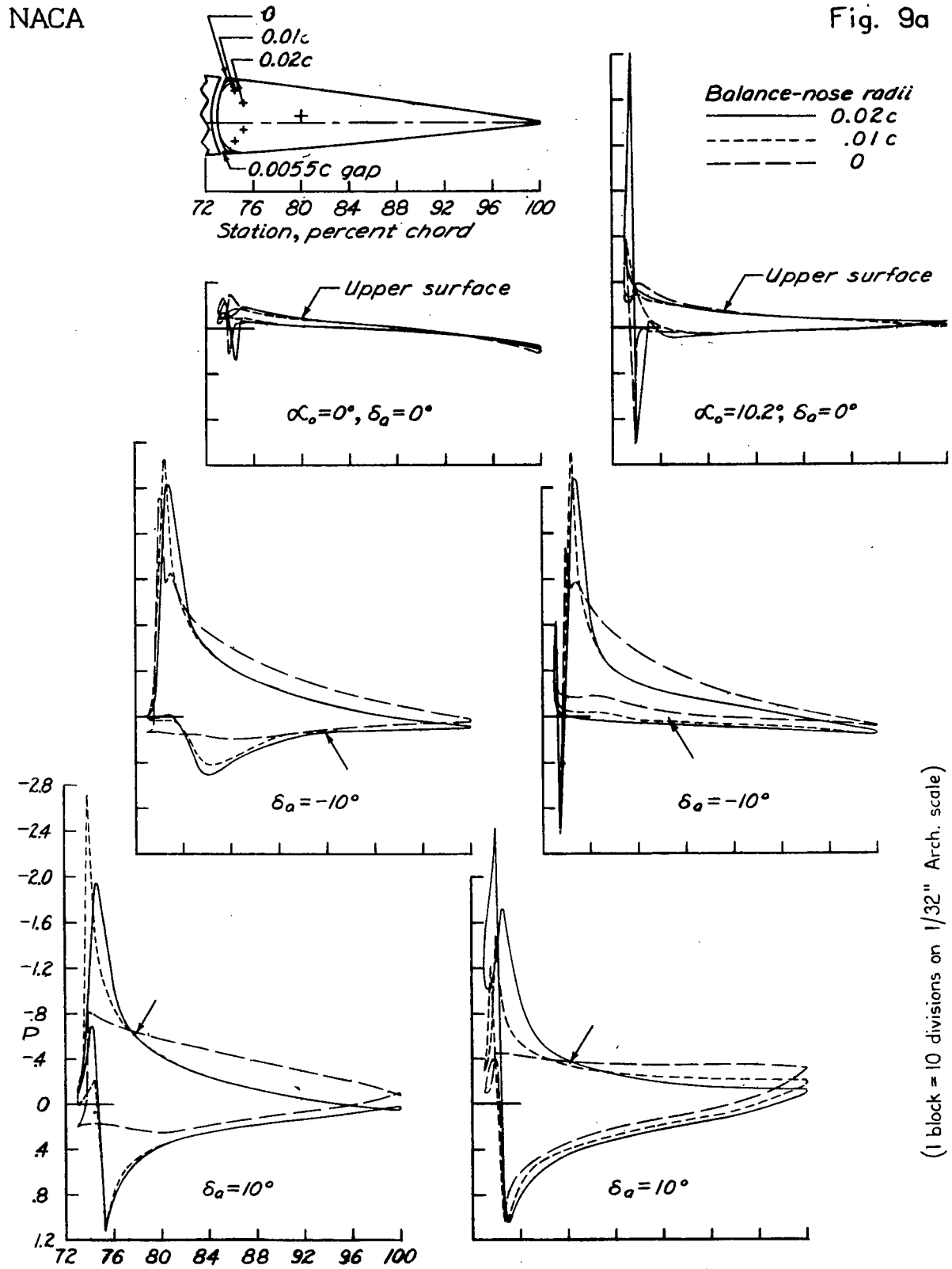

(a) Effect of balance nose radii.

Figure 9. — Pressure distribution of 0.20c aileron having a blunt-nose balance of $0.35c_a$ on the NACA 23012 airfoil. $M=0.36$.

Fig. 9b

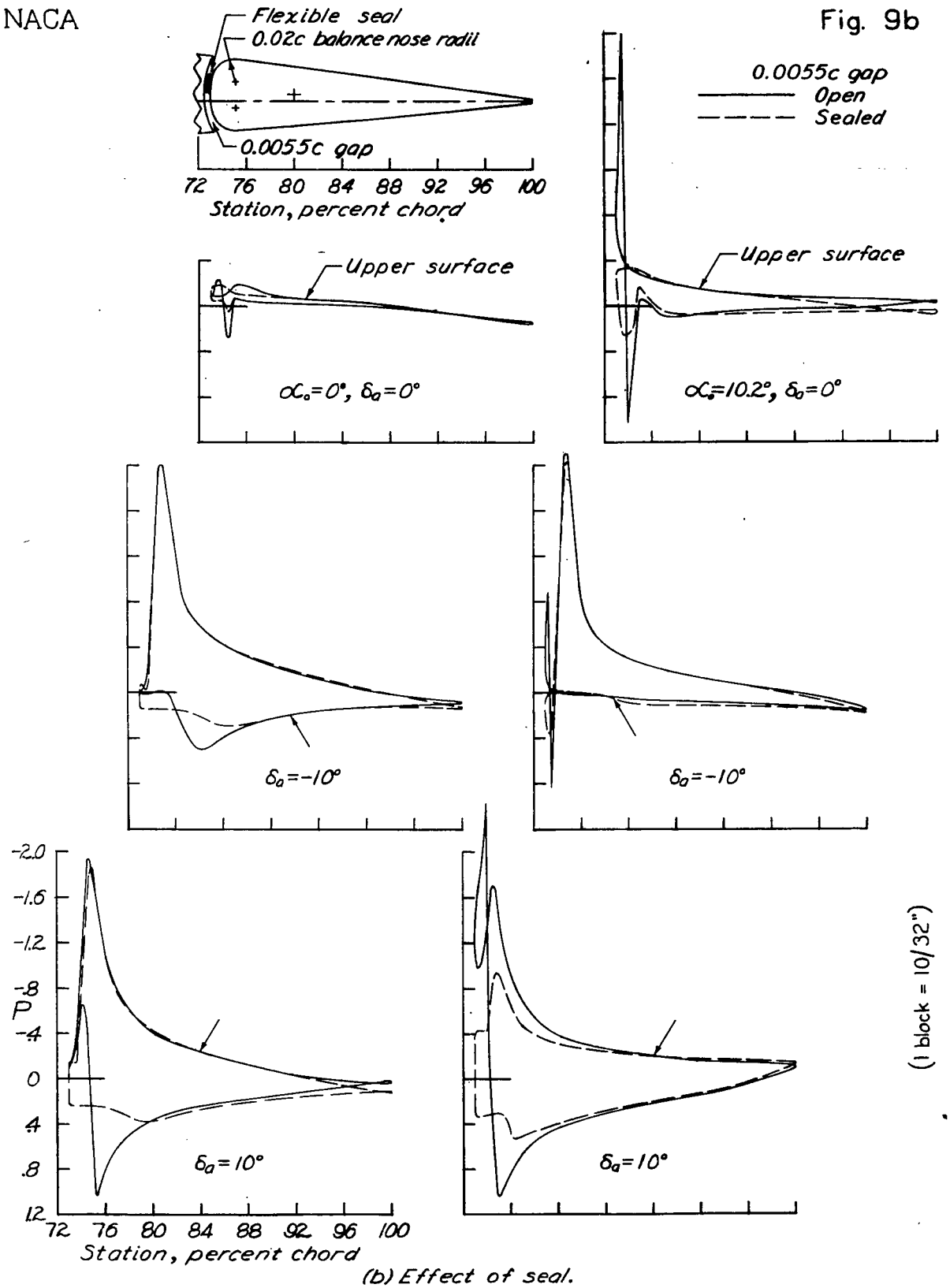

(b) Effect of seal.

Figure 9. — Concluded.

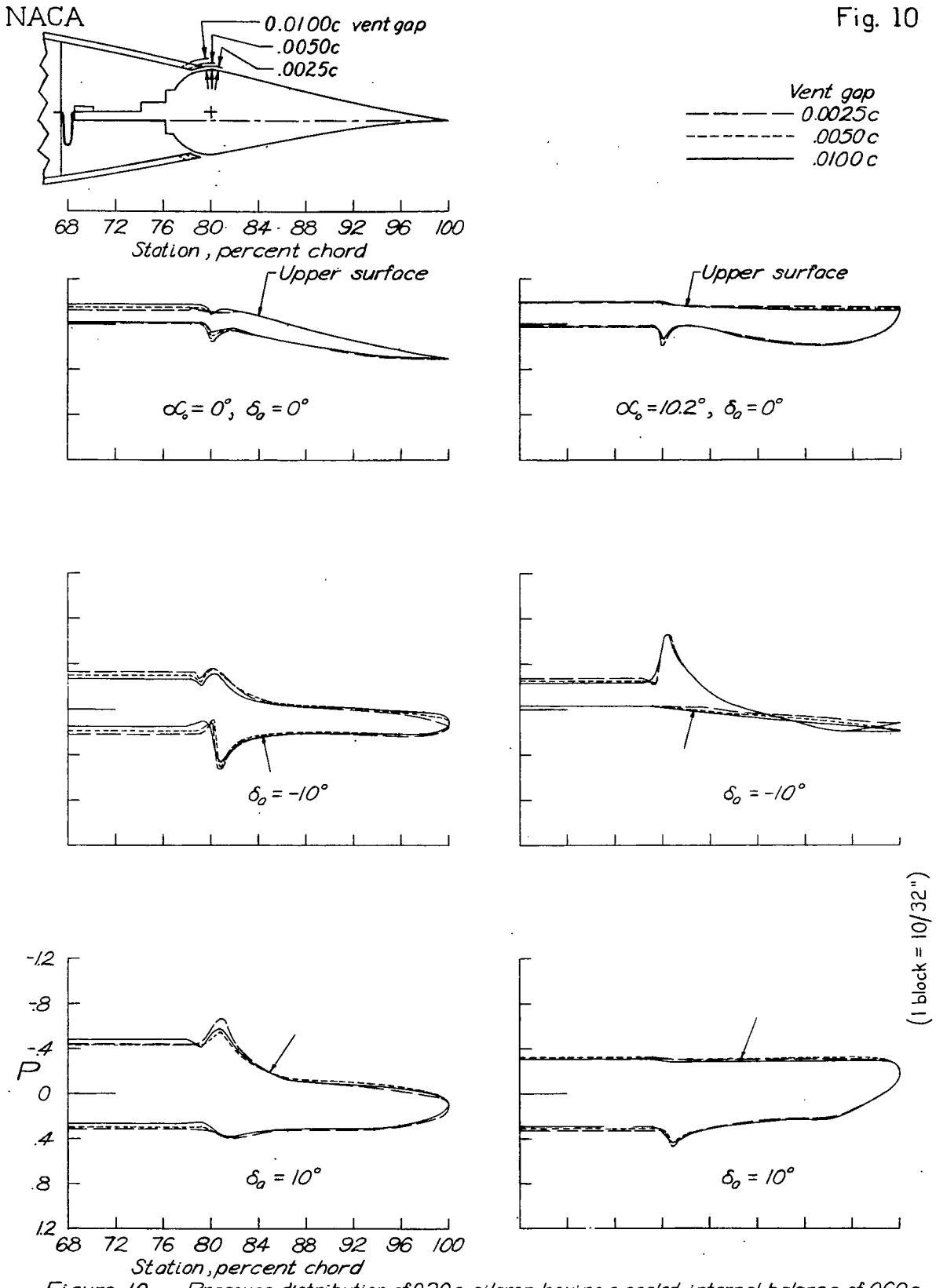

Figure 10. —Pressure distribution of 0.20c aileron having a sealed internal balance of $0.60c_a$ on the NACA 66,2-216 airfoil, showing the effect of vent gap. $M = 0.36$.

NACA

Fig. 11a

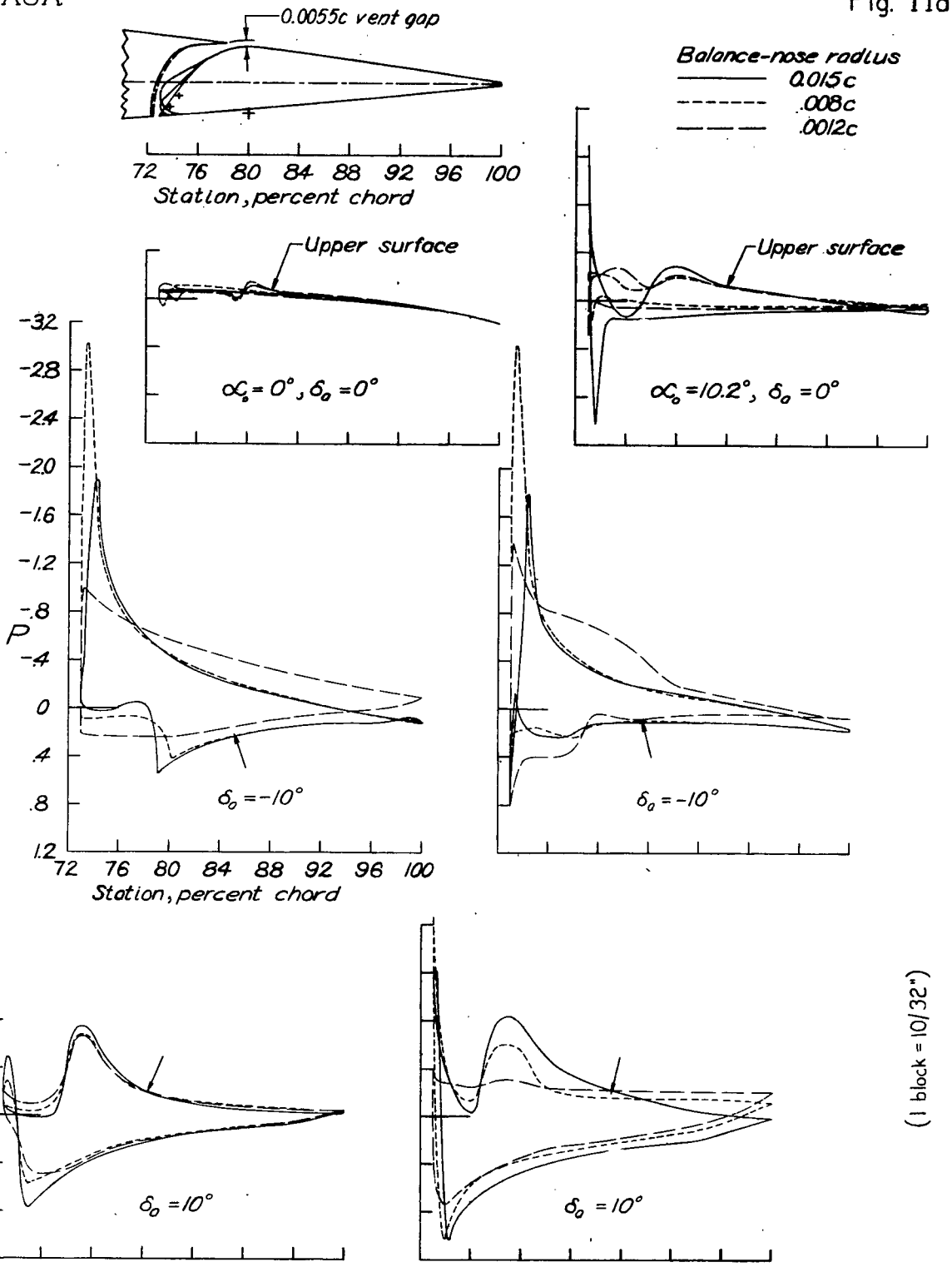

(a) Effect of balance nose radius

Figure 11. —Pressure distribution of 0.20c aileron having a Frise type balance of $0.35c_a$ on the NACA 23012 airfoil. $M = 0.36$.

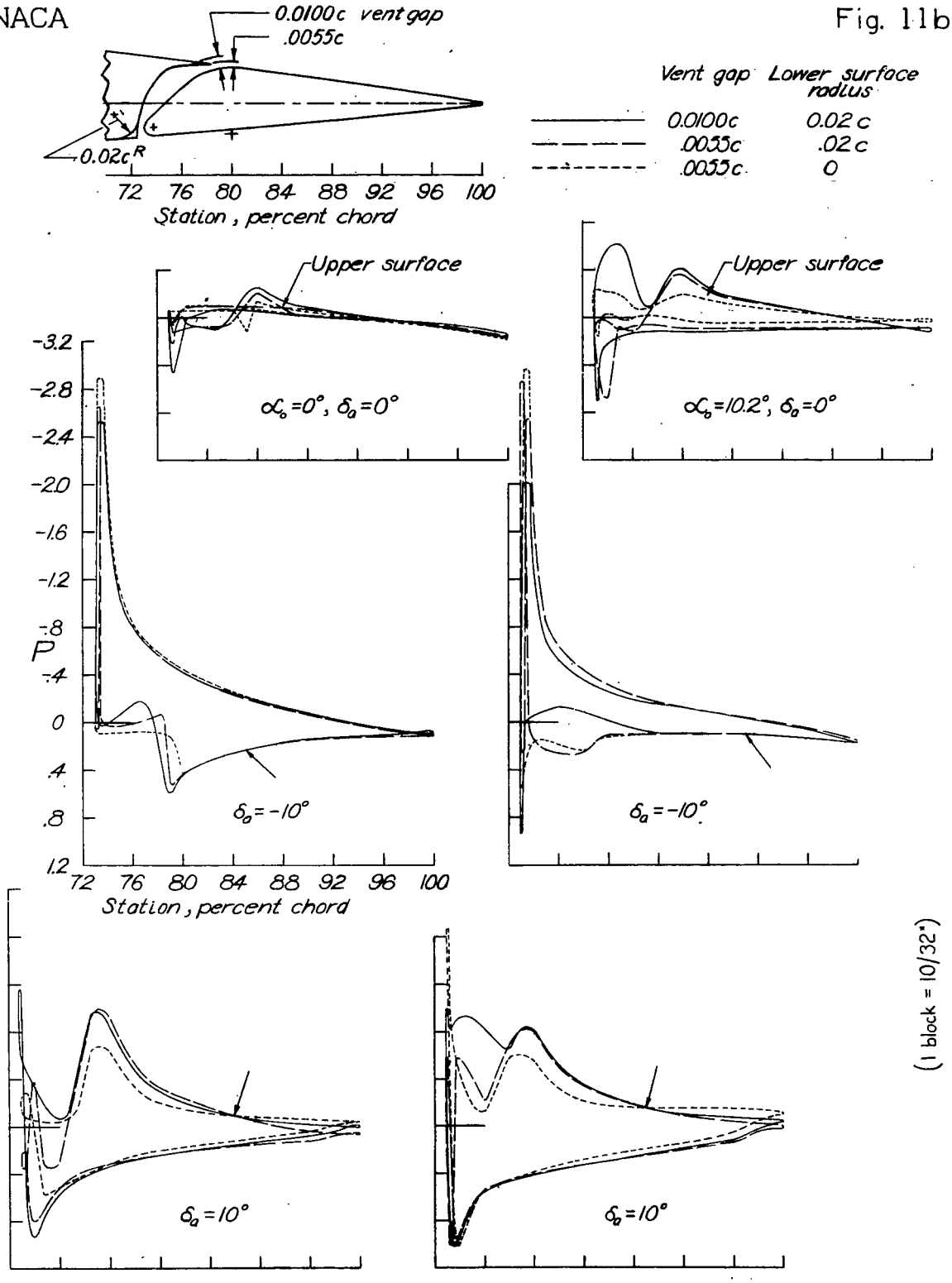

(b) Effect of vent gap and lower-surface radius. Balance-nose radius = 0.008c.

Figure 11. —Concluded.

NACA

Fig. 12a

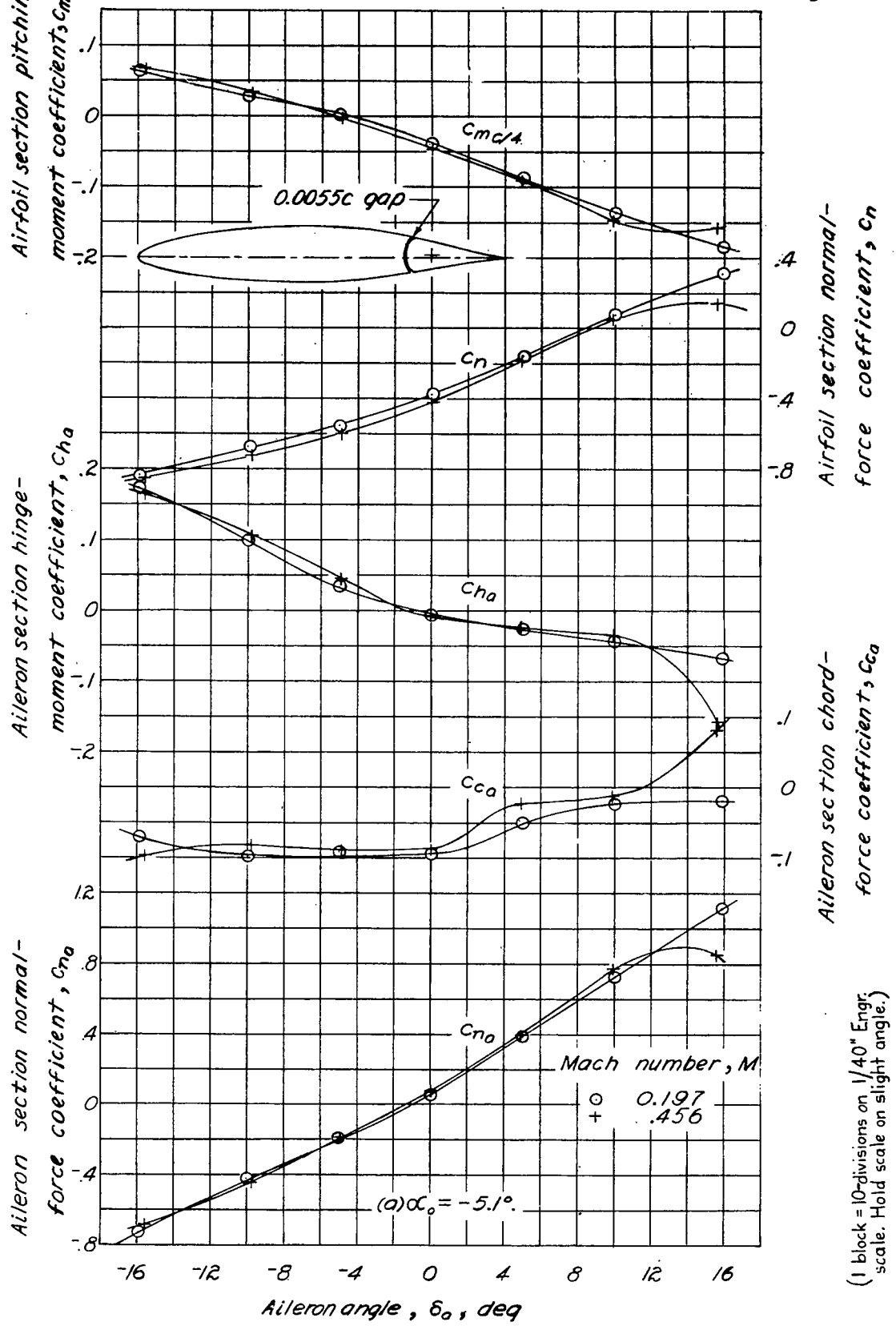

Figure 12.—Section characteristics of the NACA 66,2-216 airfoil with a 0.20c aileron having a blunt-nose balance of $0.35c_a$ and 0.02c balance-nose radii.

Fig. 12b

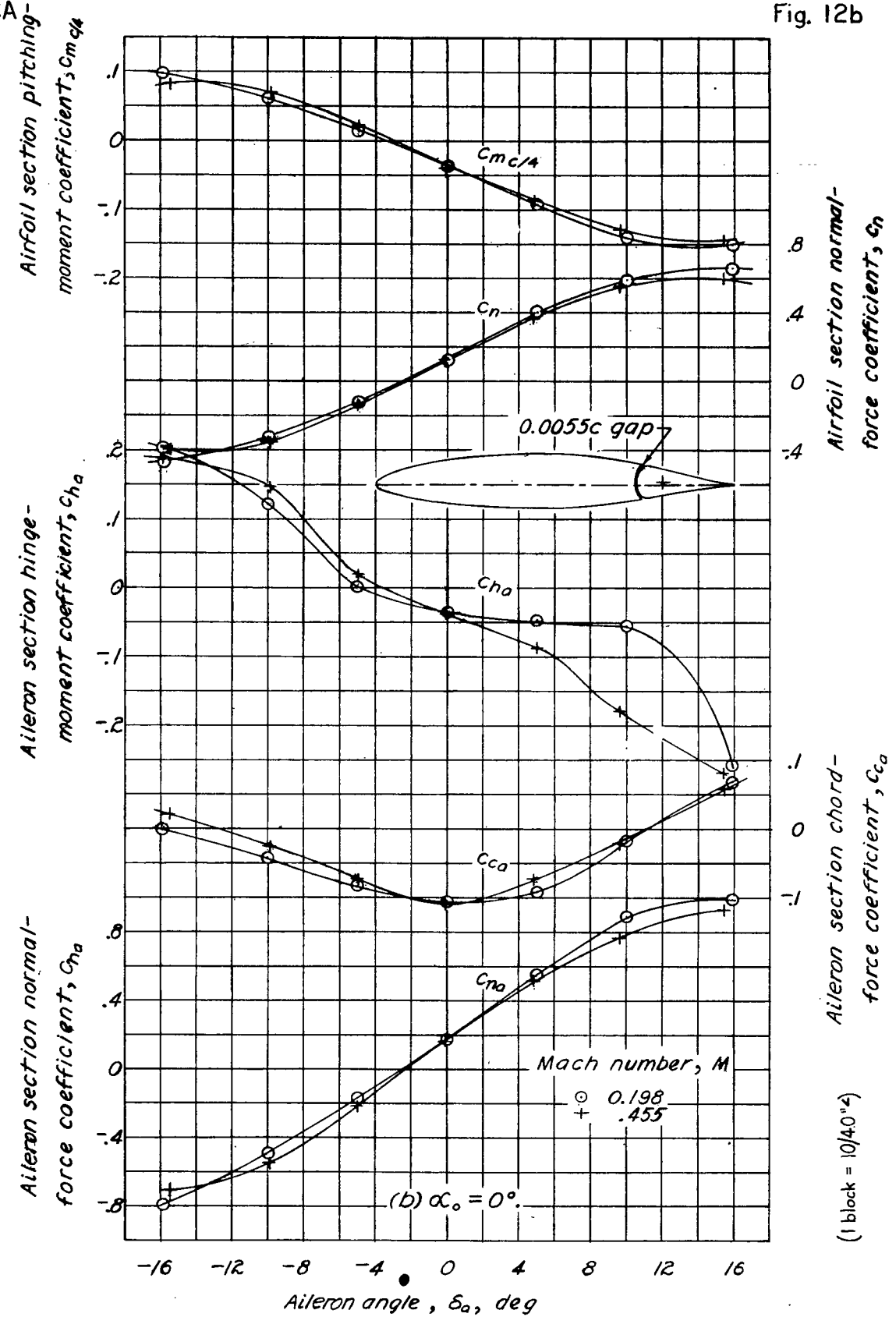

Figure 12. — Continued.

Fig. 12c

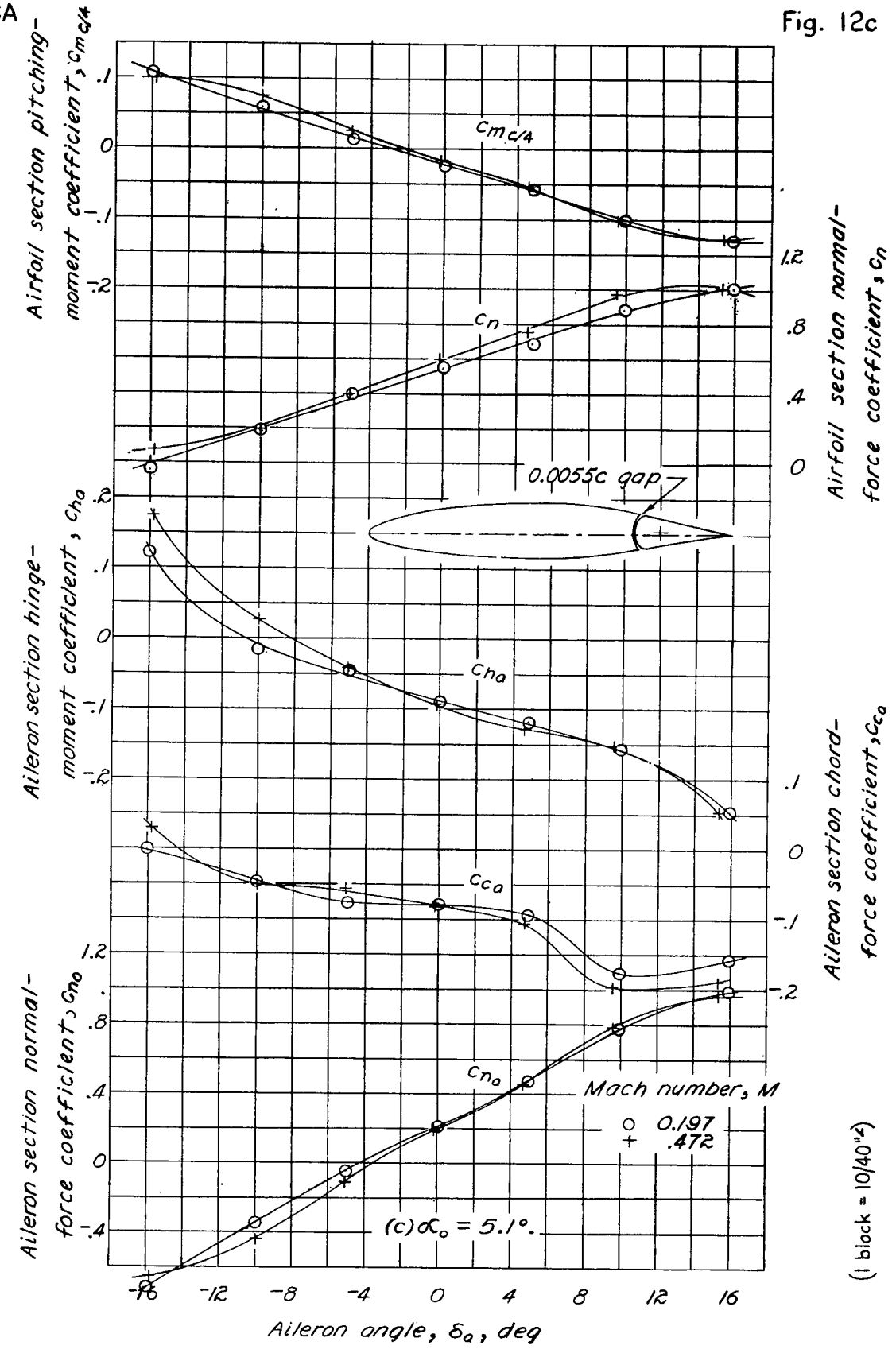

Figure 12. — Continued.

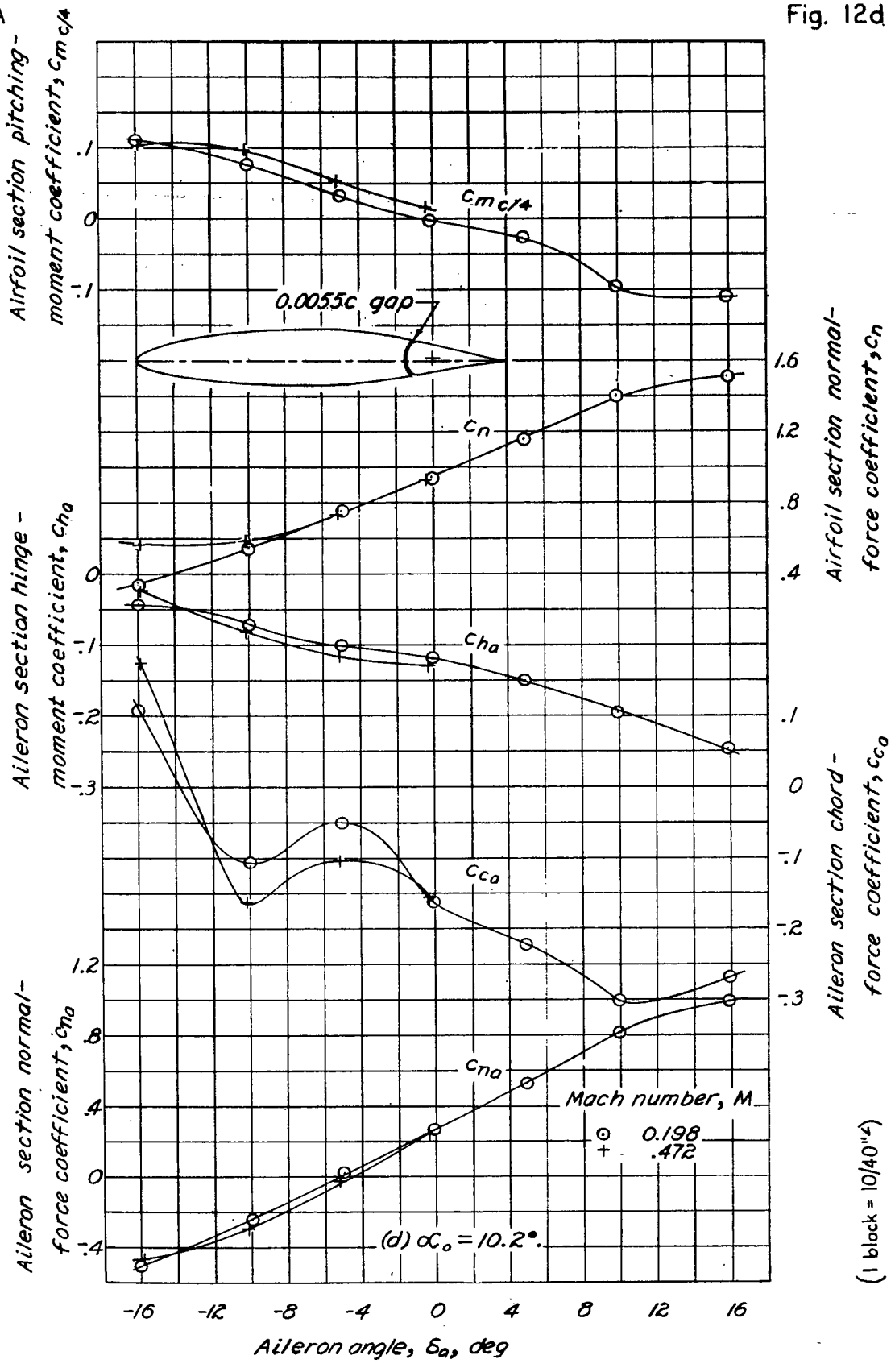

Figure 12. — Concluded.

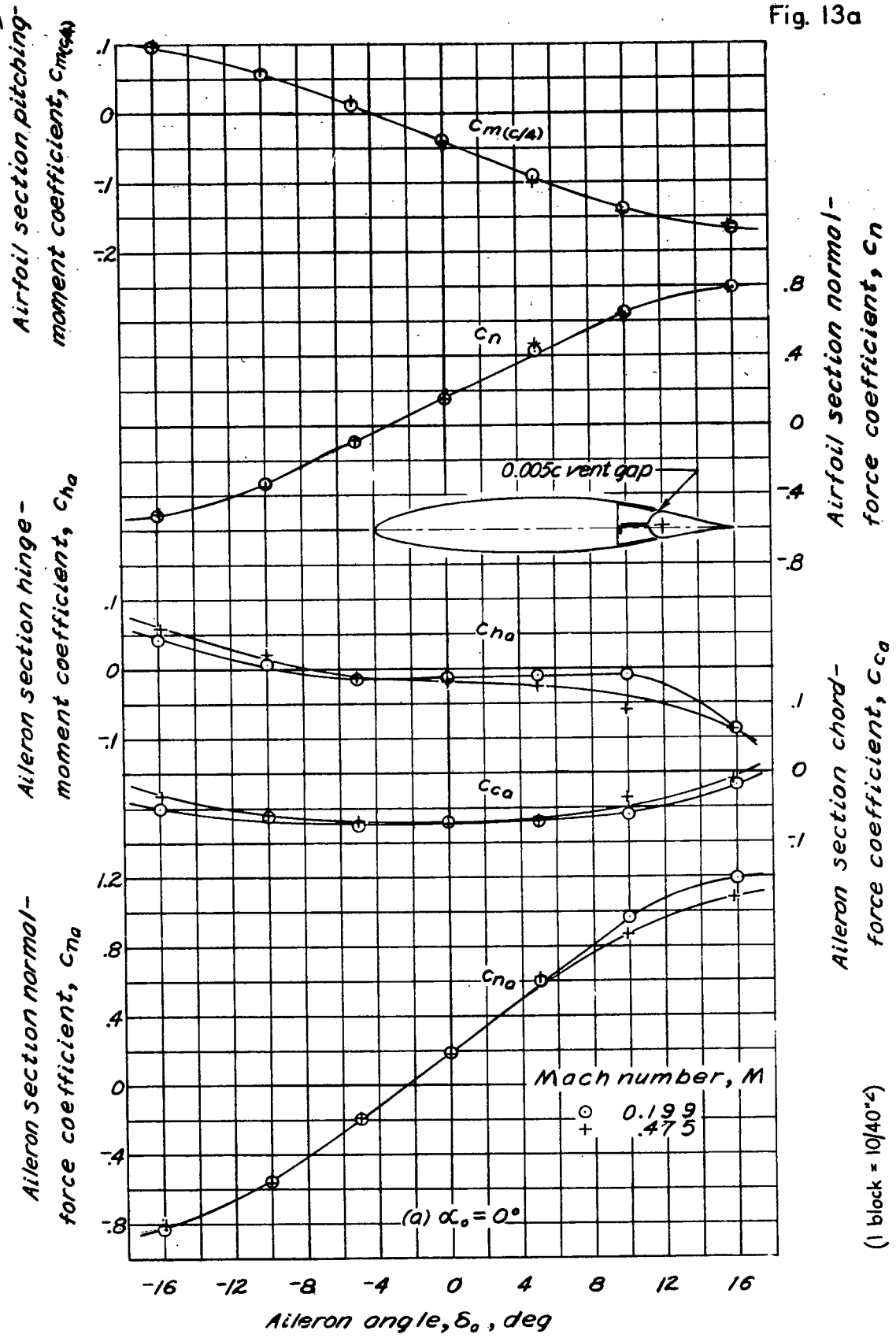

Figure 13. — Section characteristics of the NACA 66,2-216 airfoil with a 0.20c aileron having an internal balance of 0.60 c_a.

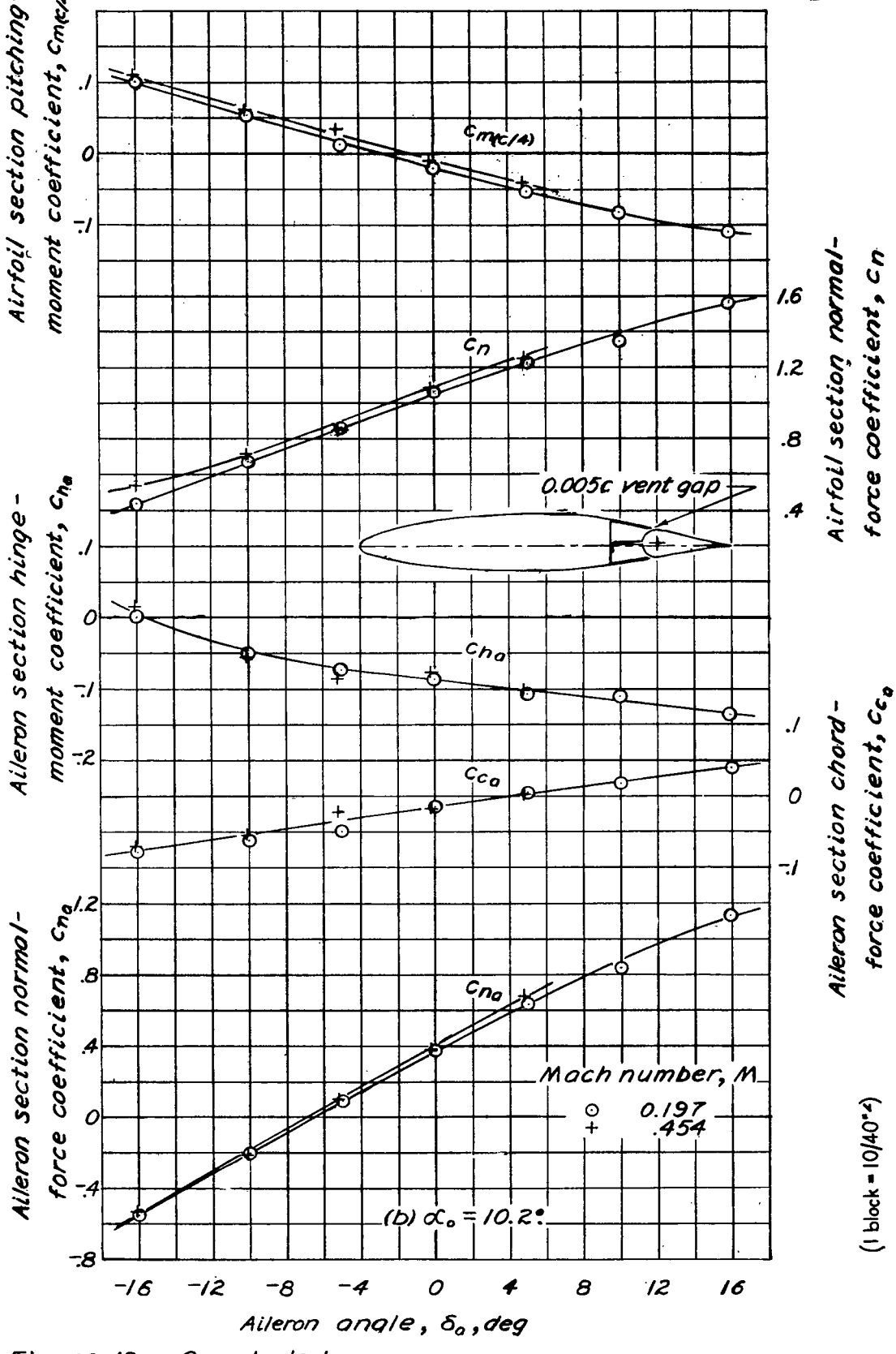

Figure 13. – Concluded.

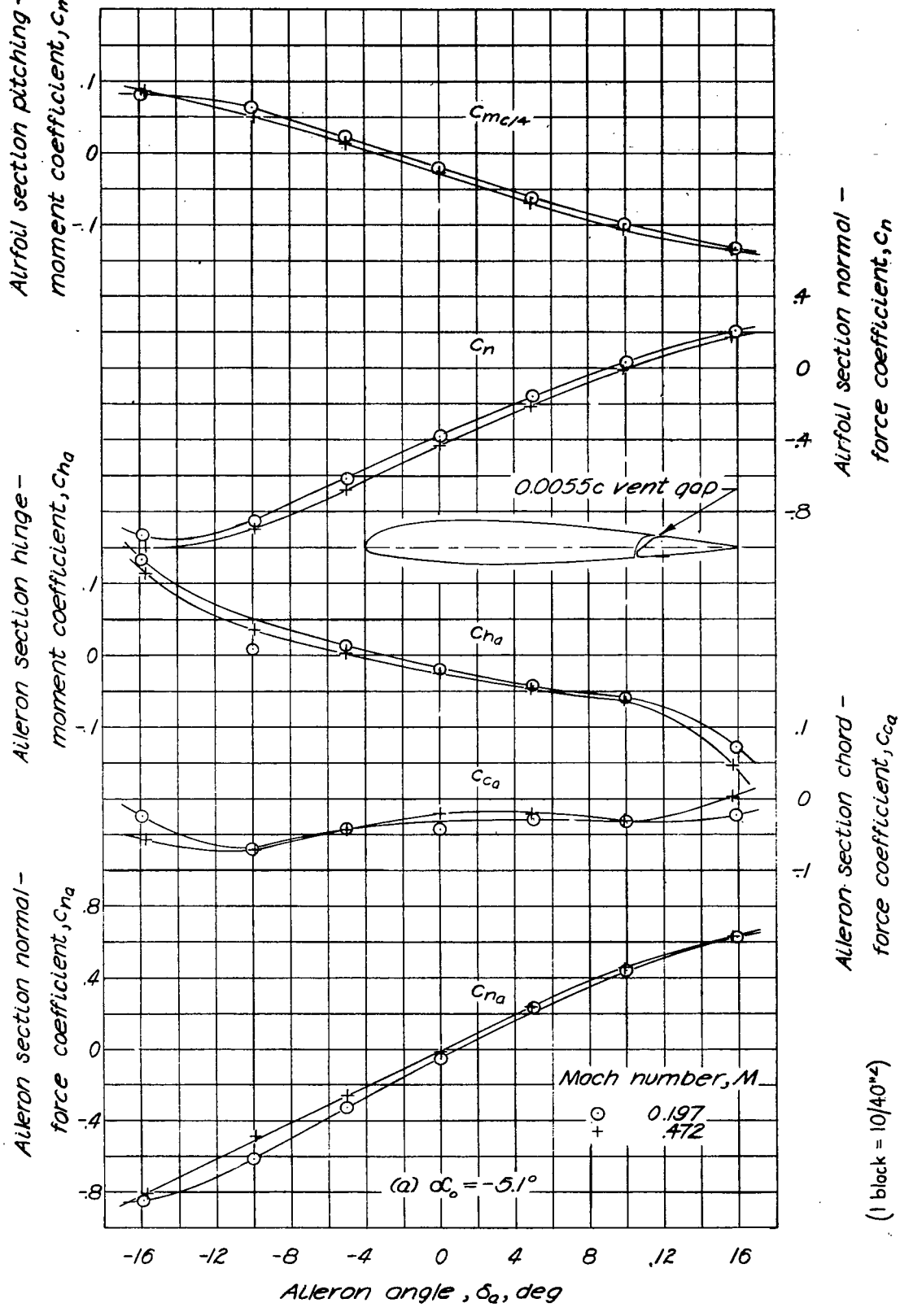

Figure 14. — Section characteristics of the NACA 23012 airfoil with a 0.20c aileron having a Frise type balance of $0.35c_a$ and a 0.008c nose radius.

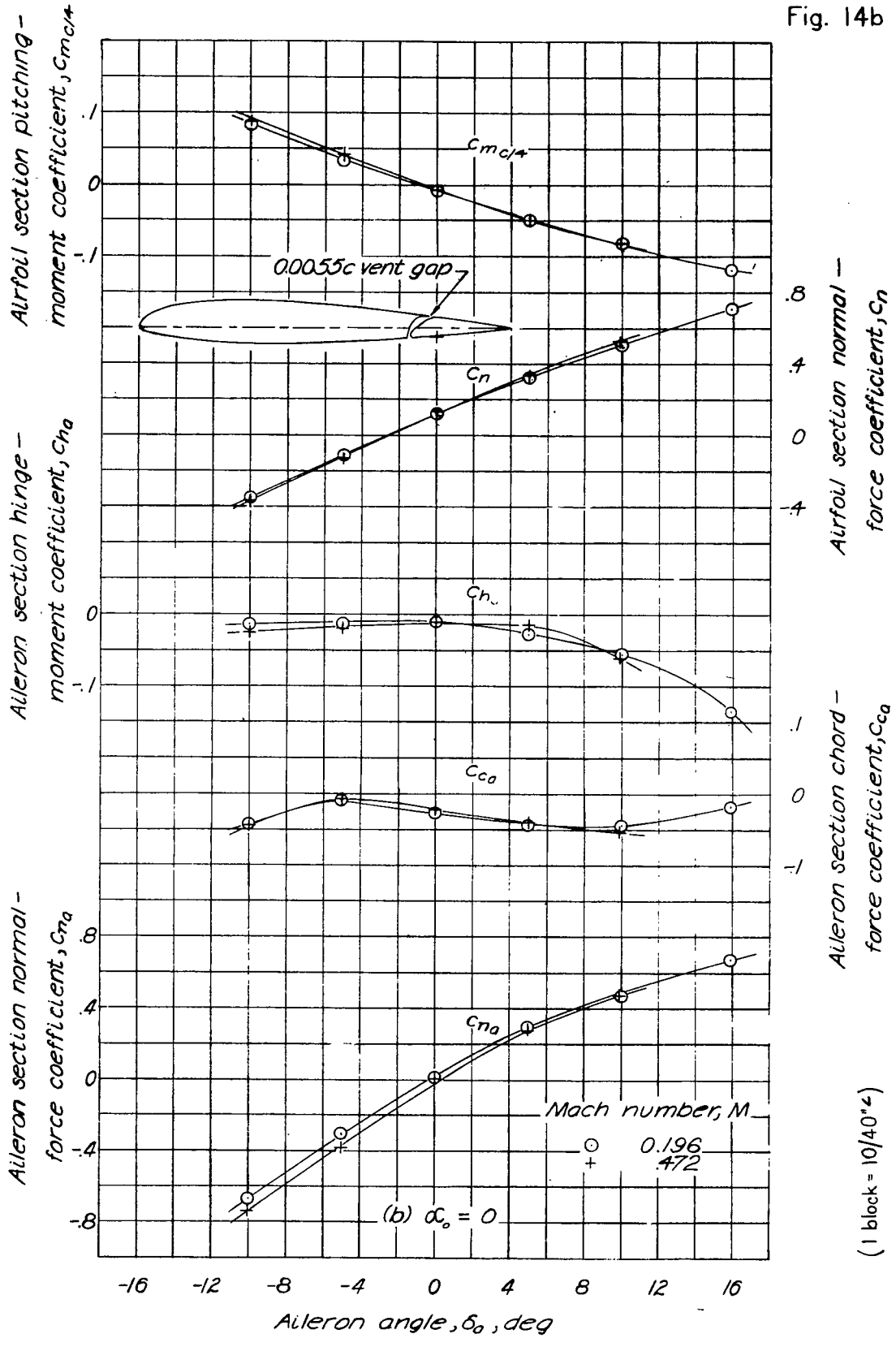

Figure 14. — Continued.

NACA

Fig. 14c

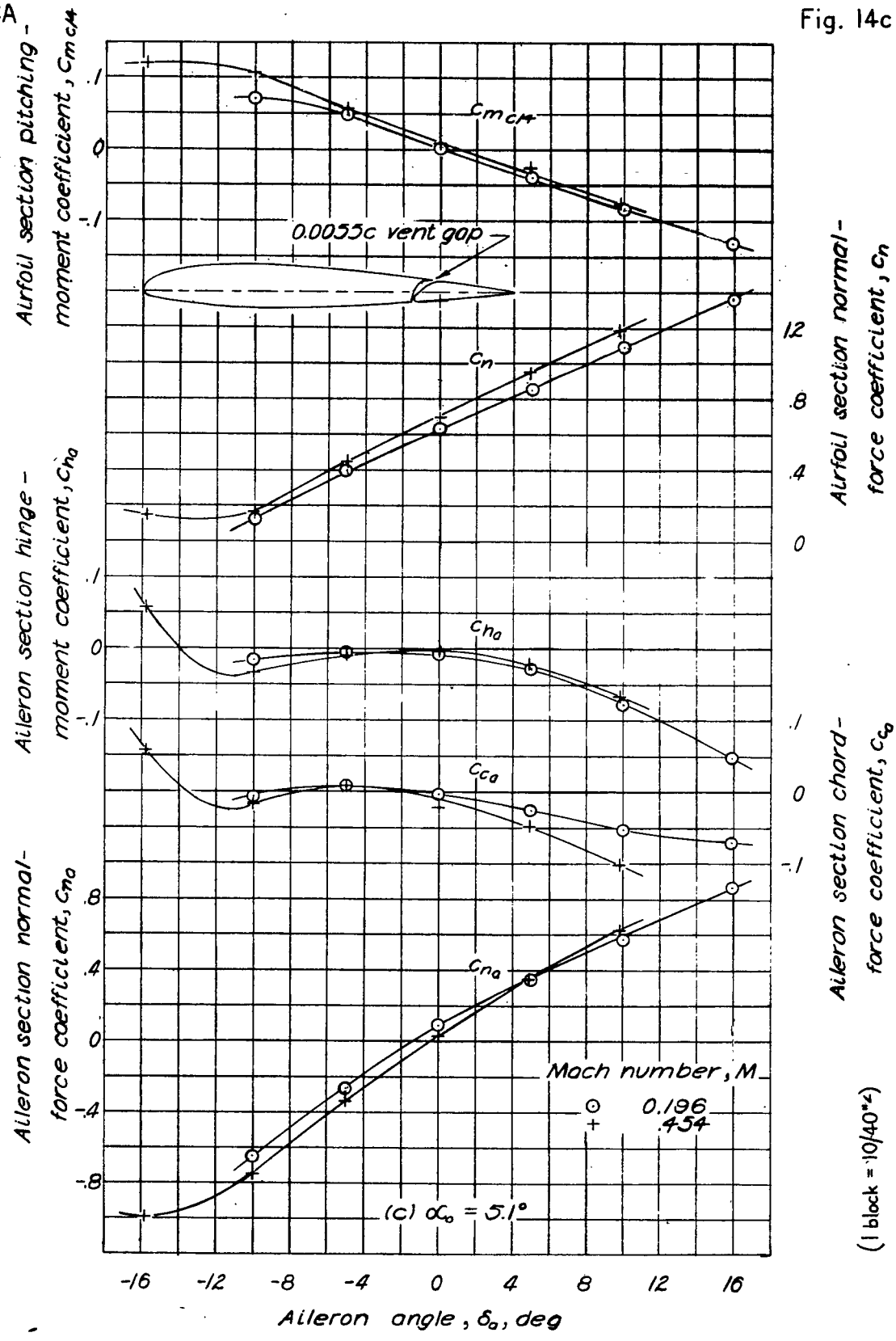

Figure 14. — Continued.

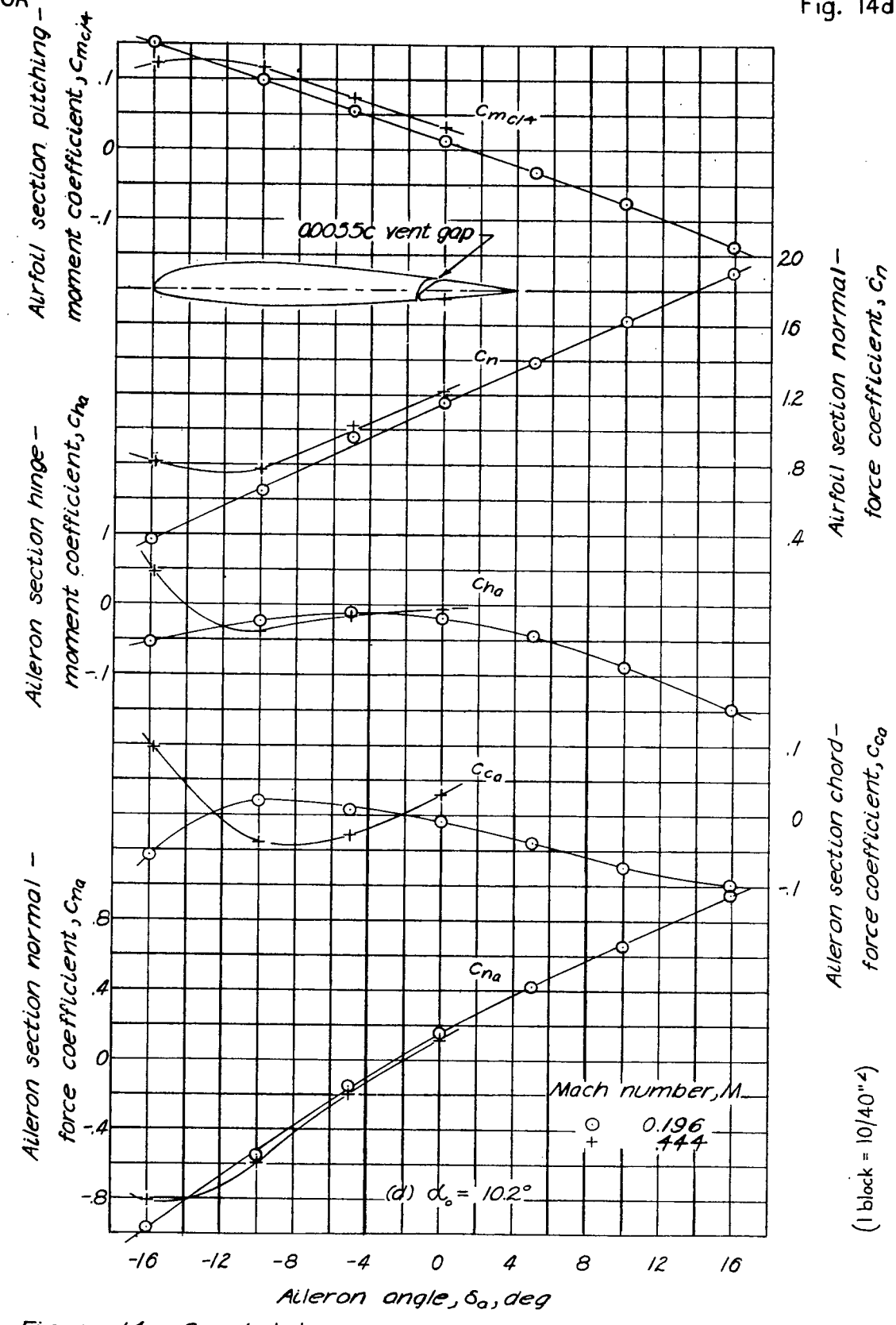

Figure 14. - Concluded.

NACA

Fig. 15a

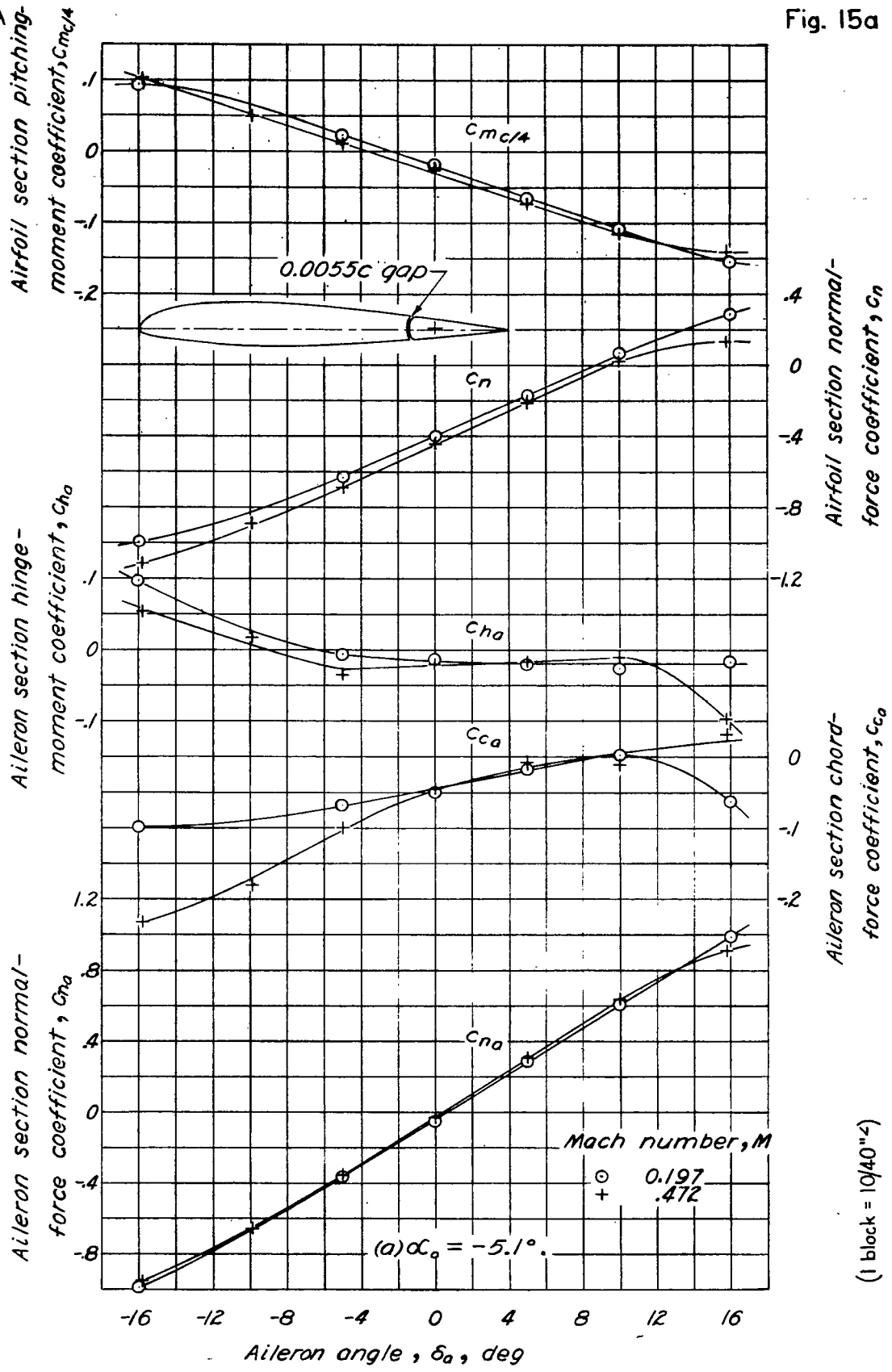

Figure 15.—Section characteristics of the NACA 23012 airfoil with a 0.20c aileron having a blunt nose balance of $0.35c_a$ and 0.02c balance-nose radii.

NACA

Fig. 15b

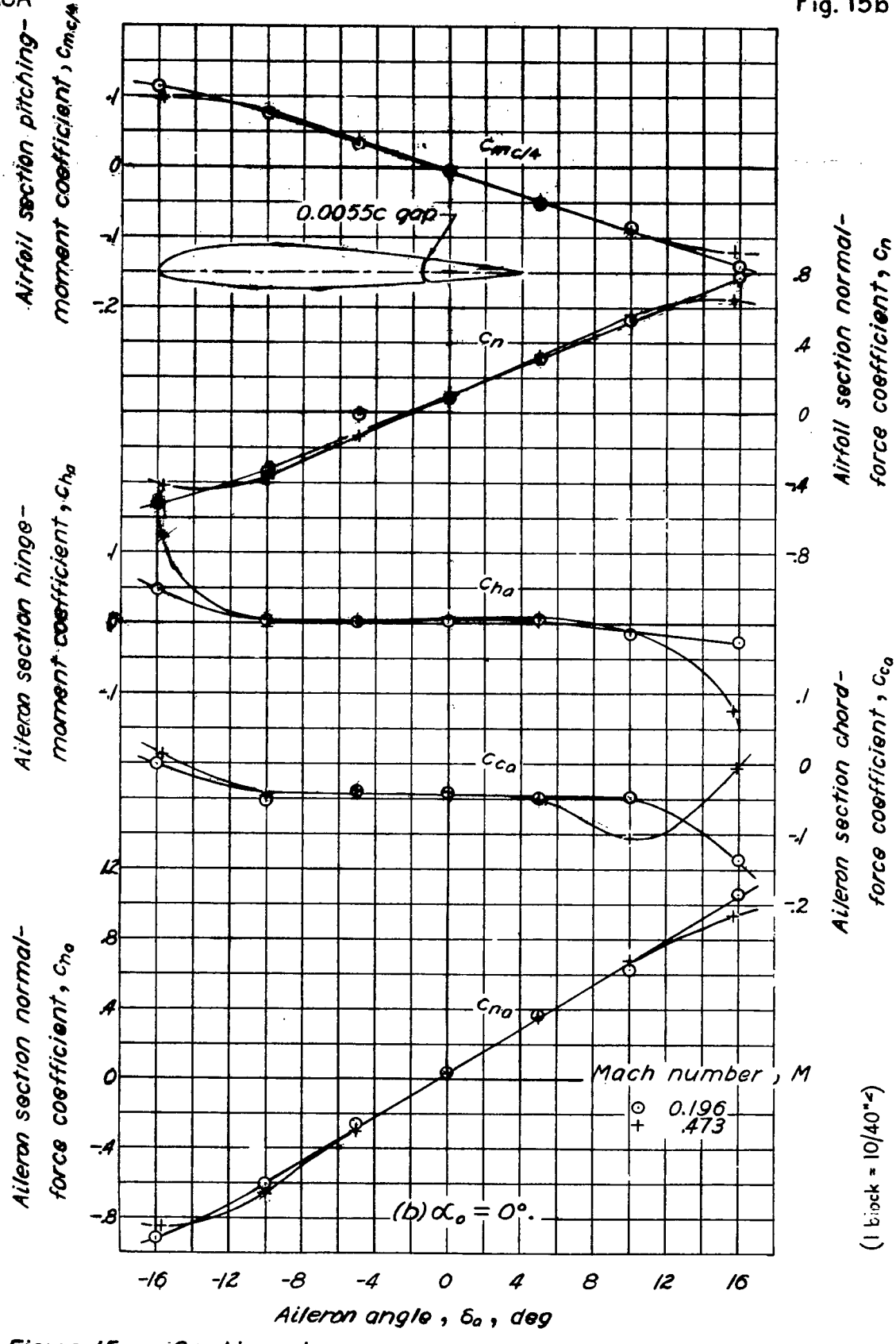

Figure 15. — Continued.

Fig. 15c

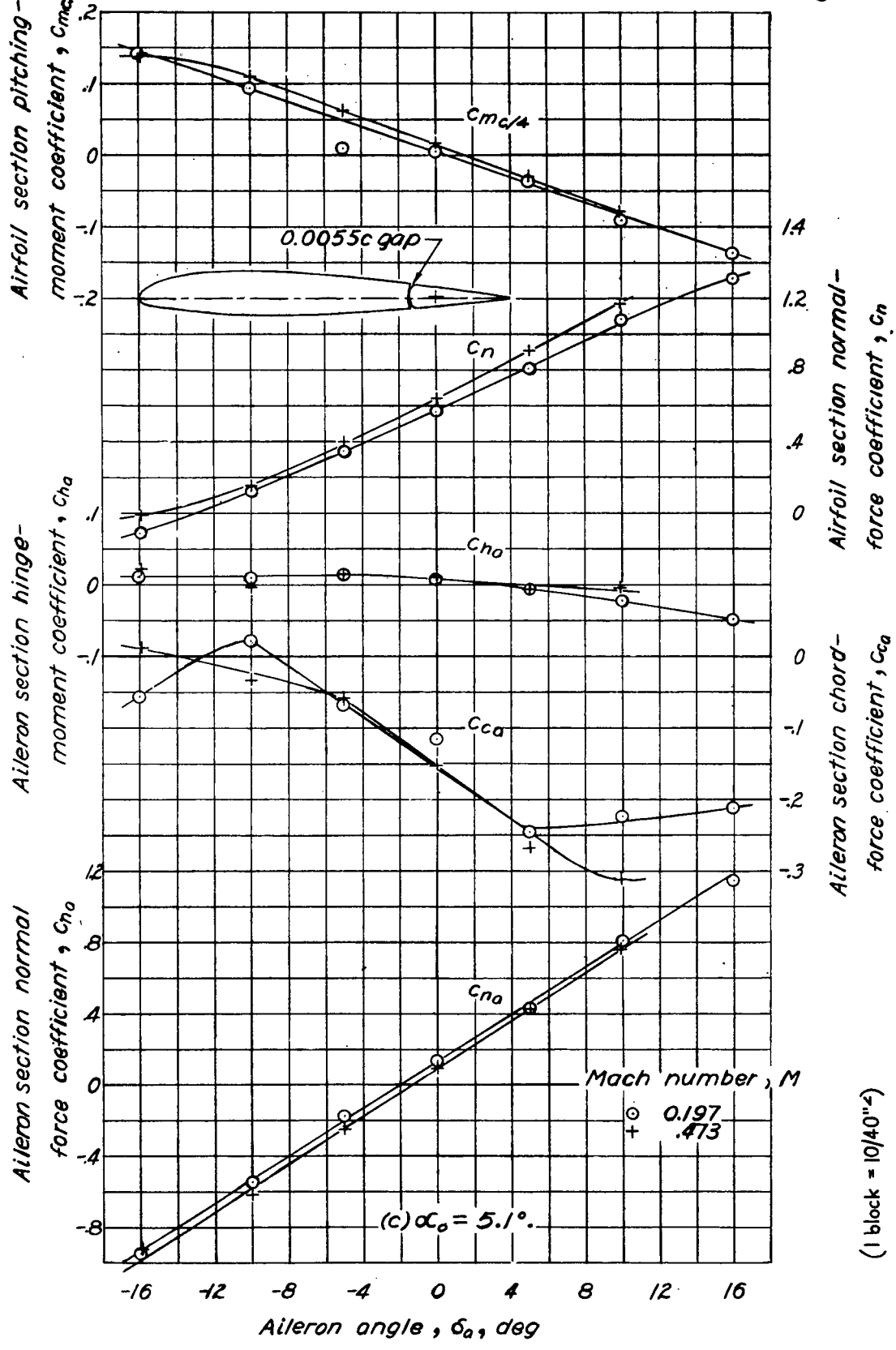

Figure 15. — Continued.

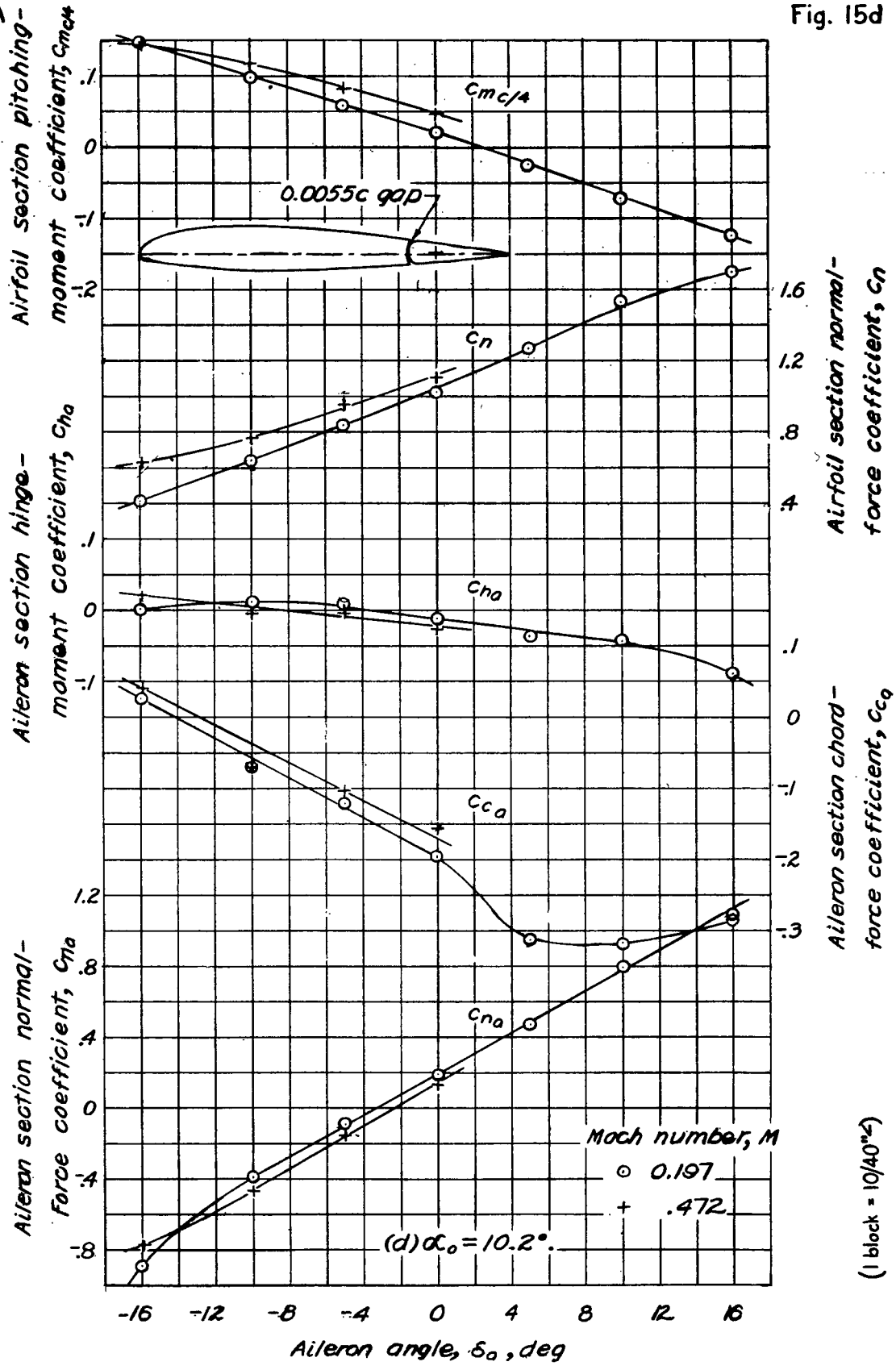

Figure 15. — Concluded.